AIMS Mathematics, 10(11): 25879–25906.
DOI:10.3934/math.20251144
Received: 25 September 2025
Revised: 27 October 2025
Accepted: 03 November 2025
Published: 10 November 2025

https://www.aimspress.com/journal/Math

Research article

Dynamic complexity in a modified Leslie-Gower model with taxis mechanism and digestion delay

Yan Meng*, Jiaxin Xiao and Caijuan Jia

School of Mathematics and Physics, University of Science and Technology Beijing, Beijing 100083, China

* **Correspondence:** Email: mengyan@ustb.edu.cn.

Abstract: In this paper, we investigate the complex spatiotemporal dynamics of a modified Leslie-Gower model with taxis mechanism and digestion delay. First, the boundedness of solutions and the global stability of the positive equilibrium point without digestion delay are obtained. Then, the occurrence conditions for Hopf bifurcation and Turing-Hopf bifurcation under the combined effect of the predator-taxis and digestion delay are obtained. Theoretically, there is no Hopf bifurcation or Turing instability as the taxis mechanism and digestion delay are absent. Our results find that the predator-taxis effect governs the existence of the Turing bifurcation and the emergence of nonhomogeneous patterns, while the digestion delay determines the stability and the existence of periodic solutions. Finally, numerical simulations verify the validity of the theoretical analysis, and homogeneous pattern, nonhomogeneous steady, nonhomogeneous periodic, and mixed patterns are observed. Interestingly, it is further shown that a double Hopf bifurcation emerges, which is induced by the interaction between nonhomogeneous Hopf bifurcations with different modes.

Keywords: Turing-Hopf bifurcation; double Hopf bifurcation; nonhomogeneous periodic pattern; predator-taxis; digestion delay
Mathematics Subject Classification: 35B32, 35B35, 35B36, 35K57

1. Introduction

Since the pioneering work of Lotka and Volterra [1, 2], interactions between predator and prey populations have been extensively studied from different mathematical perspectives [3–5]. The Leslie-Gower model is a fundamental framework for modeling predator-prey interactions, where the predator's carrying capacity is proportional to prey density [6–8]. A diffusive version of the Leslie-Gower model takes the following form:

$$\begin{cases} \dfrac{\partial u}{\partial t} - d_1\Delta u = r_1 u(1-\dfrac{u}{K}) - f(u)g(v), & x \in \Omega,\ t > 0, \\ \dfrac{\partial v}{\partial t} - d_2\Delta v = r_2(1-\dfrac{sv}{u}), & x \in \Omega,\ t > 0, \\ \dfrac{\partial u}{\partial \mathbf{n}} = \dfrac{\partial v}{\partial \mathbf{n}} = 0, & x \in \partial\Omega,\ t > 0, \\ u(x,0) = u_0(x) \geq 0, v(x,0) = v_0(x) \geq 0, & x \in \Omega, \end{cases} \tag{1.1}$$

where $u(x,t)$ and $v(x,t)$ represent the densities of prey and predator populations, respectively. $r_i(i{=}1,2)$ is the intrinsic growth rate, K represents the carrying capacity of environment, s is the maximum per capita reduction rate of predator that can be achieved, and all parameters are positive constants due to real biological meanings. $d_i(i = 1,2)$ is the diffusion coefficient, and Δ represents the Laplacian operator in $\mathbb{R}^n$. $\mathbf{n}$ is the outward unit normal vector along $\partial\Omega$, and the homogeneous Neumann boundary conditions indicate that there is no population flux across the boundaries. The term $f(u)g(v)$ represents the speed at which prey is captured. $\frac{f(u)g(v)}{v}$ means that the preys are consumed by each predators, which is referred as a functional response by Solomon [9]. Here, $f(u) = au, g(v) = \frac{v}{1+hv}$, where $a > 0$ denotes the capture rate, and $h > 0$ denotes the interference parameter among predators, which presents that the predation rate is reduced due to predators interfering with the other at high predator density. If the predator density is low, $\frac{v}{1+hv} \approx v$ for small v, and the mutual interference among predators disappears.

For the growth of a generalist predator, Upadhyay R. K. [10] modeled it as:

$$\frac{\partial v}{\partial t} - d_2\Delta v = v\left(dv - \frac{sv}{u+e}\right),$$

where d describes the growth rate of v via sexual reproduction, and e presents for other food sources to avoid a drastic reduction in the number of remaining predators due to a severe shortage of food. dv^2 signifies the fact that mating frequency is directly proportional to the number of male as well as female individuals.

In ecological environments, research shows that the spatial dynamics of population models with diffusion are more diverse [11–13]. Directed movement is ubiquitous in biological progress. Living organisms can perceive and react to their environment through moving towards or away from stimulus, the behavior is known as taxis. A typical example is predator-taxis, which means prey moves opposite to the gradient direction of predator distribution to avoid being captured by the predator. Keller and Segel [14] proposed the classical model incorporating chemotaxis, which was originally developed to illustrate the aggregation dynamics of cellular slime molds through chemical attraction. The model has served as the foundation for predator-prey models with predator-taxis [15–17]. Correspondingly, prey-taxis is defined as the directed movement that predators exhibit a tendency to migrate toward regions of high prey density for food resources. Notably, the model with prey-taxis is first proposed by Kareiva and Odell [18], which describes the non-random foraging behavior of the predator. The taxis mechanism plays a key role in exhibiting rich and complex dynamic phenomenons which either stabilize or destabilize the reaction-diffusion system under certain conditions. Chen et al. [19, 20] took the predator-taxis sensitive coefficient as a bifurcation parameter, demonstrating that attractive predator-taxis gives rise to various heterogeneous patterns and leads to the occurrence of steady-state bifurcations. Wu et al. [21] demonstrated that repulsive predator-taxis does not qualitatively affect the existence and stability of steady states, but may reduce the probability of spatial heterogeneity.

Furthermore, in most cases attractive prey-taxis tends to stabilize the interactions between predator and prey [22], while repulsive prey-taxis can give rise to pattern formation [23]. More interesting pattern formation induced by the taxis mechanism in the predator-prey system has recently been studied, see [24–26] and references therein.

Moreover, time delay exists widely in the real world. Time delay usually represents maturity period, gestation, and resource regeneration time. In the predator-prey system, when the predator consumes the prey, it will not increase the density of the predator immediately, and consumption between different populations takes some time, which is referred as digestion delay [27,28]. Many scholars have studied the effect of time delay on the predator-prey models. Song et al. [29] investigates that time delay can destabilize the positive equilibrium and induce stable spatially homogeneous periodic solutions through a delayed ratio-dependent predator-prey model. Yao et al. [30] investigated the stability and existence of the Hopf bifurcation at the coexistence equilibrium for a fear effect predator-prey model with multiple delays.

Spatial heterogeneity, which means nonhomogeneity and complexity in population spatial distribution, is universal in biological systems. While periodic phenomena, referring to periodic fluctuations in species density driven by factors such as time delay, food supply, mating habits, and harvesting, are widespread in ecosystems. It is conductive to understand the phenomenon of spatiotemporal oscillations in species density from the perspective of bifurcation. The taxis mechanism and time delay play an important role in inducing spatiotemporal nonhomogeneous patterns. Theoretically, there are no Hopf bifurcation or Turing instability as the taxis mechanism and digestion delay are absent. In fact, the taxis mechanism can induce spatially nonhomogeneous solutions, while time delay is one of the mechanisms for the existence of temporal periodic solutions. For an ecological system, it is more reasonable to consider the taxis mechanism and time delay. However, there is limited exploration in the literature for the role of the taxis sensitivity coefficient and time delay control parameter in inducing spatiotemporal nonhomogeneous patterns [31,32]. Motivated by these, we will further consider the following modified Leslie-Gower model with predator-taxis and digestion delay under homogeneous Neumann boundary conditions

$$\begin{cases} \dfrac{\partial u}{\partial t} = d_1\Delta u + \chi\nabla\cdot(u\nabla v) + ru(1-\dfrac{u}{K}) - \dfrac{auv}{1+hv}, & x\in\Omega,\ t>0,\\ \dfrac{\partial v}{\partial t} = d_2\Delta v + v(dv - \dfrac{sv}{u(x,t-\tau)+e}), & x\in\Omega,\ t>0,\\ \dfrac{\partial u}{\partial \mathbf{n}} = \dfrac{\partial v}{\partial \mathbf{n}} = 0, & x\in\partial\Omega,\ t>0,\\ u(x,0) = u_0(x)\geq 0, v(x,0) = v_0(x)\geq 0, & x\in\Omega, \end{cases} \tag{1.2}$$

where $\tau > 0$ stands for the digestion delay for the predator to convert the energy obtained from prey, and χ is the predator-taxis sensitivity parameter. The term $\chi\nabla\cdot(u\nabla v)$ describes the movement of prey toward the gradient of the predator distribution with $\chi > 0$ indicating repulsive taxis and $\chi < 0$ denoting attractive taxis, respectively.

This paper focuses on the spatiotemporal nonhomogeneous pattern phenomenon of system (1.2). By choosing the time delay control parameter and predator-taxis sensitivity coefficient as the bifurcation parameters, we obtain the sufficient conditions of the existence of the Hopf bifurcation and Turing-Hopf bifurcation. We find that the time delay control parameter determine the stability of unique

positive equilibrium and the existence of spatial homogeneous periodic solutions, and the predator-taxis sensitivity coefficient governs the existence of the Turing bifurcation and the emergence of the spatial nonhomogeneous patterns. However, the combined effect of predator-taxis and digestion delay leads to the Turing-Hopf bifurcation and the emergence of spatially nonhomogeneous periodic patterns.

The remainder of this paper is organized as follows: In Section 2, we prove the boundedness of solutions of system (1.2) and the global stability by constructing suitable Lyapunov function. In Section 3, we establish the occurrence conditions of Hopf bifurcations in system (1.2). In Section 4, the conditions for the Turing-Hopf bifurcation are given. In Section 5, numerical simulations are exhibited to illustrate the theoretical analysis and rich spatiotemporal patterns are demonstrated. Finally, a brief summary is given in Section 6.

2. Global stability and boundedness of solutions

System (1.2) has a unique positive equilibrium E_*, where

$$E_*(u_*, v_*) = (\alpha, v_\alpha),\ \alpha = \frac{s - ed}{d},\ v_\alpha = \frac{r(K-\alpha)}{aK - rh(K-\alpha)}. \tag{2.1}$$

This satisfies the following conditions:

(i) $s - ed > 0$,

(ii) $(K-\alpha)[aK - rh(K-\alpha)] > 0$.

Next, we will discuss the boundedness of solutions and the global stability of (u_*, v_*) as the digestion delay parameter $\tau = 0$.

Lemma 2.1. *Assume that $d_1, d_2, r, k, a, h, d, s$, and e are all positive, and $\Omega \subseteq \mathbb{R}^N (N \geq 1)$ is a bounded domain. Then, for $x \in \Omega, t \in (0, +\infty)$, when $rh - a > 0, s - d(K + e) > 0$ hold, we have*

$$\limsup_{t\to\infty} \max_{x\in\Omega} u(x,t) \leq K := \tilde{u}_0, \qquad \limsup_{t\to\infty} \max_{x\in\Omega} v(x,t) \leq \frac{\tilde{u}_0 + e}{s - d(\tilde{u}_0 + e)} := \tilde{v}_0,$$

$$\liminf_{t\to\infty} \min_{x\in\Omega} u(x,t) \geq K\frac{r + (rh-a)\tilde{v}_0}{r + rh\tilde{v}_0} := \hat{u}_0, \quad \liminf_{t\to\infty} \min_{x\in\Omega} v(x,t) \geq 0 := \hat{v}_0.$$

Proof. Let $(u(x,t), v(x,t))$ be a solution of system (1.2) with $u(x,0) \not\equiv 0, v(x,0) \not\equiv 0$ for $x \in \Omega$. From the first equation of system (1.2), we have

$$\frac{\partial u}{\partial t} - d_1\Delta u - \chi\nabla\cdot(u\nabla v) \leq ru\left(1 - \frac{u}{K}\right),\ x \in \Omega,\ t > 0.$$

A scalar equation with respect to u is as follows:

$$\begin{cases} \dfrac{\partial u}{\partial t} - d_1\Delta u - \chi\nabla\cdot(u\nabla v) = ru\left(1 - \dfrac{u}{K}\right), & x \in \Omega,\ t > 0, \\ \dfrac{\partial u}{\partial \mathbf{n}} = 0, & x \in \partial\Omega,\ t > 0, \\ u(x,0) = u_0(x,0), & x \in \Omega. \end{cases} \tag{2.2}$$

Let $\tilde{U}(x,t)$ be the solution of (2.2). By the comparison principle, we have $u(x,t) \leq \tilde{U}(x,t)$ for $x \in \Omega$ and $t > 0$. From $\lim_{t\to\infty} \tilde{U}(x,t) = K$ for $x \in \Omega$, we obtain

$$\limsup_{t\to\infty} \max_{x\in\Omega} u(x,t) \leq K := \tilde{u}_0.$$

For sufficiently small $\varepsilon_1 > 0$, there exists $T_1 > 0$, such that $u(x,t) \le \tilde{u}_0 + \varepsilon_1$ for $x \in \Omega$ and $t > T_1$ holds.

From the second equation of system (1.2), we have

$$\frac{\partial v}{\partial t} - d_2\Delta v \le v\left(dv - \frac{sv}{\tilde{u}_0 + \varepsilon_1 + e} + 1\right),\ x \in \Omega,\ t > T_1.$$

A scalar equation with respect to v is as follows:

$$\begin{cases} \dfrac{\partial v}{\partial t} - d_2\Delta v = v\left(dv - \dfrac{sv}{\tilde{u}_0 + \varepsilon_1 + e} + 1\right), & x \in \Omega,\ t > T_1, \\ \dfrac{\partial v}{\partial \mathbf{n}} = 0, & x \in \partial\Omega,\ t > T_1, \\ v(x, T_1) = v_0(x, T_1), & x \in \Omega. \end{cases} \tag{2.3}$$

Let $\tilde{V}(x,t)$ be the solution of (2.3). By the comparison principle, we have $v(x,t) \le \tilde{V}(x,t)$ for $x \in \Omega$ and $t > T_1$. From $\lim\limits_{t\to\infty} \tilde{V}(x,t) = \frac{\tilde{u}_0+\varepsilon_1+e}{s-d(\tilde{u}_0+\varepsilon_1+e)}$ for $x \in \Omega$ and the arbitrariness of ε_1, then as $s - d(K+e) > 0$, we obtain

$$\limsup_{t\to\infty} \max_{x\in\Omega} v(x,t) \le \frac{\tilde{u}_0 + e}{s - d(\tilde{u}_0 + e)} := \tilde{v}_0.$$

For sufficiently small $\varepsilon_2 > 0$, there exists $T_2 > T_1$ such that $v(x,t) \le \tilde{v}_0 + \varepsilon_2$ for $x \in \Omega$ and $t > T_2$ holds.

From the first equation of system (1.2), we have

$$\frac{\partial u}{\partial t} - d_1\Delta u - \chi\nabla\cdot(u\nabla v) \ge ru\left(1 - \frac{u}{K}\right) - \frac{au}{\frac{1}{\tilde{v}_0+\varepsilon_2} + h},\ x \in \Omega,\ t > T_2.$$

A scalar equation with respect to u is as follows:

$$\begin{cases} \dfrac{\partial u}{\partial t} - d_1\Delta u - \chi\nabla\cdot(u\nabla v) = ru\left(1 - \dfrac{u}{K}\right) - \dfrac{au(\tilde{v}_0 + \varepsilon_2)}{1 + h(\tilde{v}_0 + \varepsilon_2)}, & x \in \Omega,\ t > T_2, \\ \dfrac{\partial u}{\partial \mathbf{n}} = 0, & x \in \partial\Omega,\ t > T_2, \\ u(x, T_2) = u_0(x, T_2), & x \in \Omega. \end{cases} \tag{2.4}$$

Let $\hat{U}(x,t)$ be the solution of (2.4). By the comparison principle, we have $u(x,t) \ge \hat{U}(x,t)$ for $x \in \Omega$ and $t > T_2$. Then, as $rh - a > 0$, from $\lim\limits_{t\to\infty} \tilde{U}(x,t) = K\frac{r+(\tilde{v}_0+\varepsilon_2)(rh-a)}{r+rh(\tilde{v}_0+\varepsilon_2)}$ for $x \in \Omega$ and the arbitrariness of ε_2, we obtain

$$\liminf_{t\to\infty} \min_{x\in\Omega} u(x,t) \ge K\frac{r + \tilde{v}_0(rh - a)}{r + rh\tilde{v}_0} := \hat{u}_0.$$

From the second equation of system (1.2), we have

$$\begin{cases} \dfrac{\partial v}{\partial t} - d_2\Delta v = v\left(dv - \dfrac{sv}{u + e}\right), & x \in \Omega,\ t > 0, \\ \dfrac{\partial v}{\partial \mathbf{n}} = 0, & x \in \partial\Omega,\ t > 0, \\ v(x, 0) = v_0(x, 0), & x \in \Omega. \end{cases} \tag{2.5}$$

As such, treating (2.5) as a scalar equation with respect to v, we find that zero is a lower solution to (2.5). Thus, we obtain

$$\liminf_{t\to\infty} \min_{x\in\Omega} v(x,t) \ge 0 := \hat{v}_0.$$

The proof is complete. □

Remark 2.1. *From Lemma 2.1, we know that the limit set of all solutions* (u, v) *of system* (1.2) *belongs to* $G_0 = [X_1, X_2] \times [Y_1, Y_2]$*, where*

$$X_1 = \min\{\hat{u}_0, \min u_0(x)\}, \quad X_2 = \max\{\tilde{u}_0, \max u_0(x)\},$$
$$Y_1 = \min\{\hat{v}_0, \min v_0(x)\}, \quad Y_2 = \max\{\tilde{v}_0, \max v_0(x)\}.$$

That is, we have proved that solutions of system (1.2) *are bounded under certain conditions. Next, we prove the global stability of the positive steady state* (u_*, v_*) *of system* (1.2) *without time delay by using a Lyapunov function.*

Theorem 2.1. *Assume that* $d_1, d_2, r, k, a, h, d, s$*, and* e *are all positive, and Lemma 2.1 holds. The coexistence equilibrium* $E_* = (u_*, v_*)$ *is globally asymptotically stable for* $(u, v) \in G_0 = [X_1, X_2] \times [Y_1, Y_2]$ *and system* (1.2) *without delay if* (H_1) *and* (H_2) *hold, where*

$$(H_1): \chi^2 < \frac{4d_1d_2v_*}{u_*Y_2^2}, \ \frac{r}{K} > d,$$

$$(H_2): d < \frac{s}{X_2 + e} - \frac{K}{r}\left[\frac{a}{2(1 + hY_1)(1 + hv_*)} - \frac{sv_*}{2(X_2 + e)(u_* + e)}\right]^2.$$

Proof. Using the Lyapunov function

$$V(t) = \int_\Omega \left(u - u_* - u_* \ln \frac{u}{u_*}\right) dx + \int_\Omega \left(v - v_* - v_* \ln \frac{v}{v_*}\right) dx,$$

the derivative of $V(t)$ is

$$\begin{aligned}
\dot{V}(t) &= \int_\Omega \left(\frac{u - u_*}{u}\right) \frac{\partial u}{\partial t} dx + \int_\Omega \left(\frac{v - v_*}{v}\right) \frac{\partial v}{\partial t} dx \\
&= \int_\Omega \left(\frac{u - u_*}{u}\right) (d_1 \Delta u + \chi \nabla \cdot (u \nabla v)) dx + \int_\Omega d_2 \left(\frac{u - u_*}{u}\right) \Delta v dx \\
&\quad + \int_\Omega (u - u_*) \left[r\left(1 - \frac{u}{K}\right) - \frac{av}{1 + hv}\right] dx + \int_\Omega (v - v_*) \left(dv - \frac{sv}{u + e}\right) dx \\
&= V_1 + V_2.
\end{aligned}$$

On the one hand, we denote

$$\begin{aligned}
V_1 &= \int_\Omega \left(\frac{u - u_*}{u}\right) (d_1 \Delta u + \chi \nabla \cdot (u \nabla v)) dx + \int_\Omega d_2 \left(\frac{u - u_*}{u}\right) \Delta v dx \\
&= -\int_\Omega \left[\frac{d_1 u_*}{u^2} |\nabla u|^2 + \frac{d_2 v_*}{v^2} |\nabla v|^2 + \frac{\chi u_*}{u^2} \nabla u \cdot \nabla v\right] dx \\
&= -\int_\Omega P_1^T Q_1 P_1 dx.
\end{aligned}$$

Define

$$P_1 = \begin{pmatrix} \nabla u \\ \nabla v \end{pmatrix}, Q_1 = \begin{pmatrix} \frac{d_1 u_*}{u^2} & \frac{\chi u_*}{2u} \\ \frac{\chi u_*}{2u} & \frac{d_2 v_*}{v^2} \end{pmatrix}.$$

Then,

$$Trace(Q_1) = \frac{d_1 u_*}{u^2} + \frac{d_2 v_*}{v^2} > 0, Det(Q_1) = \frac{d_1 d_2 u_* v_*}{u^2 v^2} - \frac{\chi^2 u_*^2}{4u^2}.$$

Therefore, $Det(Q_1) > 0$ is equivalent to $\chi^2 < \frac{4d_1 d_2 v_*}{u_* v^2}$. One finds that it means

$$\chi^2 < \frac{4d_1 d_2 v_*}{u_* Y_2^2},$$

because of $Y_1 \le v(x,t) \le Y_2$. Therefore, Q_1 is a positive definite matrix, implying that $V_1 \le 0$.

On the other hand, we denote

$$\begin{aligned}
V_2 &= \int_\Omega (u-u_*)\left[r\left(1-\frac{u}{K}\right) - \frac{av}{1+hv}\right]dx + \int_\Omega (v-v_*)\left(dv - \frac{sv}{u+e}\right)dx \\
&= \int_\Omega (u-u_*)\left[r - \frac{r(u-u_*)}{K} - \frac{ru_*}{K} - \frac{a(v-v_*)}{1+hv} - \frac{av_*}{1+hv}\right]dx \\
&\quad + \int_\Omega (v-v_*)\left[d(v-v_*) + dv_* - \frac{s(v-v_*)}{u+e} - \frac{sv_*}{u+e}\right]dx \\
&= -\int_\Omega (u-u_*)^2 \frac{r}{K}dx - \int_\Omega (v-v_*)^2\left(\frac{s}{u+e} - d\right)dx \\
&\quad - \int_\Omega (u-u_*)(v-v_*)\left[\frac{a}{(1+hv)(1+hv_*)} - \frac{sv_*}{(u+e)(u_*+e)}\right]dx \\
&= -\int_\Omega P_2^T Q_2 P_2 dx,
\end{aligned}$$

where

$$P_2 = \begin{pmatrix} u-u_* \\ v-v_* \end{pmatrix}, Q_2 = \begin{pmatrix} \frac{r}{K} & \frac{a}{2(1+hv)(1+hv_*)} - \frac{sv_*}{2(u+e)(u_*+e)} \\ \frac{a}{2(1+hv)(1+hv_*)} - \frac{sv_*}{2(u+e)(u_*+e)} & \frac{s}{u+e} - d \end{pmatrix}.$$

Thus,

$$Trace(Q_2) = \frac{r}{K} + \frac{s}{u+e} - d,$$

$$Det(Q_2) = \frac{r}{K}\left(\frac{s}{u+e} - d\right) - \left[\frac{a}{2(1+hv)(1+hv_*)} - \frac{sv_*}{2(u+e)(u_*+e)}\right]^2.$$

We obtain $Trace(Q_2) > 0$ if

$$\frac{r}{K} - d > 0.$$

In addition, if we suppose

$$d < \frac{s}{u+e} - \frac{K}{r}\left[\frac{a}{2(1+hv)(1+hv_*)} - \frac{sv_*}{2(u+e)(u_*+e)}\right]^2,$$

one obtains $Det(Q_2) > 0$. Noting that $X_1 \le u(x,t) \le X_2$ and $Y_1 \le v(x,t) \le Y_2$, we have

$$d < \frac{s}{X_2+e} - \frac{K}{r}\left[\frac{a}{2(1+hY_1)(1+hv_*)} - \frac{sv_*}{2(X_2+e)(u_*+e)}\right]^2.$$

Then, Q_2 is a positive definite matrix, implying that $V_2 \le 0$.

To sum up, we obtain $\dot{V}(t) = V_1 + V_2 \le 0$. Thus, the positive steady state $E_* = (u_*, v_*)$ is globally stable for $(u,v) \in G_0 = [X_1, X_2] \times [Y_1, Y_2]$ and system (1.2) without delay. The proof is complete. □

3. Hopf bifurcation

In this section, we investigate the Hopf bifurcation of system (1.2). We linearize system (1.2) at the coexistence equilibrium E_* and obtain

$$\begin{pmatrix} \frac{\partial u}{\partial t} \\ \frac{\partial v}{\partial t} \end{pmatrix} = \begin{pmatrix} d_1\frac{\partial^2}{\partial x^2} & \chi\alpha\frac{\partial^2}{\partial x^2} \\ 0 & d_2\frac{\partial^2}{\partial x^2} \end{pmatrix}\begin{pmatrix} u \\ v \end{pmatrix} + A_0\begin{pmatrix} u \\ v \end{pmatrix} + A_\tau\begin{pmatrix} u_\tau \\ v_\tau \end{pmatrix}, \tag{3.1}$$

where

$$A_0 = \begin{pmatrix} a_1 & a_2 \\ 0 & 0 \end{pmatrix}, A_\tau = \begin{pmatrix} 0 & 0 \\ b & 0 \end{pmatrix}.$$

From (2.1), $\alpha = u_* > 0$, so

$$a_1 = -\frac{r\alpha}{K} < 0,\ a_2 = -\frac{a\alpha}{(1+hv_*)^2} < 0,\ b = \frac{sv_*^2}{(\alpha+e)^2} > 0. \tag{3.2}$$

Subsequently, the characteristic equation of system (3.1) is

$$\det(\mu I + M_{\mathrm{n}} - A_0 - A_\tau e^{-\mu\tau}) = 0, \tag{3.3}$$

where I is the 2×2 identity matrix, $\mathrm{M}_n = \begin{pmatrix} d_1\lambda_n & \chi\alpha\lambda_n \\ 0 & d_2\lambda_n \end{pmatrix}$, and $\lambda_n = \frac{n^2}{l^2}$ is the eigenvalue of $-\Delta$ under Neumann boundary conditions with $n \in \mathbb{N}_0$. From (3.3), we obtain the following equation:

$$\mu^2 + (d_1\lambda_n + d_2\lambda_n - a_1)\mu + d_1d_2\lambda_n^2 - d_2\lambda_n a_1 + (\chi\alpha\lambda_n - a_2)be^{-\mu\tau} = 0. \tag{3.4}$$

Substituting $\mu = 0$ into Eq (3.4), we obtain

$$d_1d_2\lambda_n^2 + (-d_2a_1 + \chi\alpha b)\lambda_n - a_2b = 0. \tag{3.5}$$

There is no $\lambda_n > 0$ satisfying Eq (3.5) due to all the coefficients of Eq (3.5) being positive, which indicates that system (1.2) does not undergo the steady state bifurcation.

In the following, we focus on the analysis of Hopf bifurcations. For $\tau > 0$, we substitute $\mu = i\omega_n$ ($\omega_n > 0$) into (3.4) and obtain

$$-\omega_n^2 + (d_1\lambda_n + d_2\lambda_n - a_1)i\omega_n + d_1d_2\lambda_n^2 - d_2\lambda_n a_1 + (\chi\alpha\lambda_n - a_2)be^{-i\omega_n\tau} = 0,$$

that is,

$$e^{-i\omega_n\tau} = \frac{\omega_n^2 - (d_1\lambda_n + d_2\lambda_n - a_1)i\omega_n - d_1d_2\lambda_n^2 + d_2\lambda_n a_1}{(\chi\alpha\lambda_n - a_2)b}. \tag{3.6}$$

For $e^{-i\omega_n\tau} = \cos(\omega_n\tau) - i\sin(\omega_n\tau)$, separating the real and imaginary parts of the Eq (3.6), we obtain

$$\begin{cases} \cos(\omega_n\tau) = \dfrac{\omega_n^2 - d_1d_2\lambda_n^2 + d_2\lambda_n a_1}{(\chi\alpha\lambda_n - a_2)b}, \\ \sin(\omega_n\tau) = \dfrac{(d_1\lambda_n + d_2\lambda_n - a_1)\omega_n}{(\chi\alpha\lambda_n - a_2)b}. \end{cases} \tag{3.7}$$

We have

$$\omega_n^4 + \left[(d_1\lambda_n - a_1)^2 + d_2^2\lambda_n^2\right]\omega_n^2 + (d_1d_2\lambda_n^2 - d_2\lambda_n a_1)^2 - (\chi\alpha\lambda_n - a_2)^2b^2 = 0. \tag{3.8}$$

Since $(d_1\lambda_n - a_1)^2 + d_2^2\lambda_n^2 > 0$, then Eq (3.8) has positive roots when

$$(d_1d_2\lambda_n^2 - d_2\lambda_n a_1)^2 - (\chi\alpha\lambda_n - a_2)^2b^2 < 0,$$

which implies that

$$d_1d_2\lambda_n^2 - (\chi\alpha b + d_2a_1)\lambda_n + a_2b < 0. \tag{3.9}$$

Next, we present Lemmas 3.1 and 3.2 to analyze the occurrence of a Hopf bifurcation in system (1.2).

Lemma 3.1. *Let*

$$\xi(\chi) = \frac{1}{2d_1d_2}\left[(d_2a_1 + \chi\alpha b) + \sqrt{(d_2a_1 + \chi\alpha b)^2 - 4d_1d_2a_2b}\right], \tag{3.10}$$

and

$$\chi_* = \begin{cases} \dfrac{1}{\alpha b l^2}\left(d_1d_2 - d_2a_1l^2 + a_2bl^4\right), & 0 < l \le l_0, \\ 0, & l > l_0, \end{cases} \tag{3.11}$$

where

$$l_0 = \sqrt{\frac{1}{2a_2b}\left(d_2a_1 - \sqrt{d_2^2a_1^2 - 4d_1d_2a_2b}\right)}. \tag{3.12}$$

Then, we have

(*i*) *if* $0 < \chi \le \chi_*$, *there is a pair of pure imaginary roots* $\pm i\omega_0$ *for the characteristic Eq* (3.4) *at* $\tau = \tau_{0j}$ *with*

$$\tau_{0j} = \frac{1}{\omega_0}\left[\arccos\left(\frac{\omega_0^2}{-a_2b}\right) + 2j\pi\right],\ j \in \mathbb{N}_0; \tag{3.13}$$

(*ii*) *if* $\chi > \chi_*$, *there is a pair of pure imaginary roots* $\pm i\omega_n$ $(0 \le n \le N)$ *for the characteristic Eq* (3.4) *at* $\tau = \tau_{nj}$ *with*

$$\tau_{nj} = \frac{1}{\omega_n}\left[\arccos\left(\frac{\omega_n^2 - d_1d_2\lambda_n^2 + d_2\lambda_n a_1}{(\chi\alpha\lambda_n - a_2)b}\right) + 2j\pi\right],\ j \in \mathbb{N}_0, \tag{3.14}$$

where $N = \left[\sqrt{\xi(\chi)l^2}\right]$ *and* $[\cdot]$ *denotes the integer part function.*

Proof. Considering Eq (3.8) as a quadratic function of ω^2, it exhibits positive roots when inequality (3.9) holds. To study the distribution of roots corresponding to inequality (3.9), by letting $p = \lambda_n$, we obtain

$$d_1d_2p^2 - (\chi\alpha b + d_2a_1)p + a_2b = 0. \tag{3.15}$$

It is clear that Eq (3.15) has a unique positive root $p = \xi(\chi)$ defined by (3.10). To ensure that Eq (3.8) with $n \ge 1$ has positive roots, there must exist λ_n for $n \ge 1$ to satisfy (3.9). Since λ_n is monotonically increasing, that is, $\lambda_1 < \lambda_2 < \cdots < \lambda_n < \cdots$, we obtain that if λ_1 does not satisfy (3.9), implying $\lambda_1 > \xi(\chi)$, then all λ_n do not satisfy (3.9). It is shown that Eq (3.8) does not have a positive root for $n \ge 1$.

When $\chi = 0$, $\xi(\chi)$ takes its minimum value as follows:

$$\xi(0) = \min_{\chi \geq 0} \xi(\chi) = \frac{1}{2d_1d_2}\left(d_2a_1 + \sqrt{d_2^2a_1^2 - 4d_1d_2a_2b}\right).$$

By solving $\lambda_1|_{l=l_0} = \frac{1}{l_0^2} = \xi(0)$, which is equivalent to

$$\frac{d_1d_2}{l_0^4} - \frac{d_2a_1}{l_0^2} + ba_2 = 0,$$

then we obtain l_0 in (3.12). When $l > l_0$, it implies that $\lambda_1 = \frac{1}{l^2} < \frac{1}{l_0^2}$ and $\frac{1}{l_0{}^2} = \xi(0)$. We deduce that $\lambda_1 = \frac{1}{l^2} < \min_{\chi>0} \xi(\chi)$, so there exists $n \geq 1$ such that Eq (3.8) has solutions for $\chi > 0$. In this case, the critical value χ of Eq (3.8) is $\chi_* = 0$.

When $0 < l \leq l_0$, assuming the critical value of Eq (3.8) is χ_*, and considering $\lambda_1 = \frac{1}{l^2} = \xi(\chi_*)$, we solve the equation as follows:

$$\frac{1}{l^2} = \frac{1}{2a_2b}\left(d_2a_1 + \alpha b\chi_* + \sqrt{(d_2a_1 + \alpha b\chi_*)^2 - 4d_1d_2a_2b}\right).$$

Then, we obtain

$$\chi_* = \frac{1}{\alpha b l^2}\left(d_1d_2 - d_2a_1l^2 + a_2bl^4\right).$$

Clearly, when $0 < \chi \leq \chi_*$, there exists no $n \geq 1$ satisfying $\lambda_n < \xi(\chi)$. Therefore, there is no $\omega_{\rm n} > 0$ such that Eq (3.8) has solutions. When $\chi > \chi_*$, there is λ_1 that satisfies inequality (3.9). This means that when $n \geq 1$, there must be certain values λ_n satisfying (3.9).

Next, we assume $\lambda_N < \xi(\chi)$ to obtain the number of solutions for (3.9), then we obtain the number of solutions as $N = \left[\sqrt{\xi(\chi)l^2}\right]$. Furthermore, the stability of positive equilibrium is determined by the first critical value of the Hopf bifurcation. By solving Eq (3.7), the critical value is $\tau = \tau_{nj}$ for $0 \leq n \leq N$ as in (3.14). This completes the proof. □

Lemma 3.2. *τ_{00} and $\tau_{n0}(\chi)$ are defined by* (3.13) *and* (3.14) *with $j = 0$ as follows:*

$$\begin{cases} \tau_{00} = \dfrac{1}{\omega_0}\arccos\left(\dfrac{\omega_0^2}{-a_2b}\right), \\ \tau_{n0} = \dfrac{1}{\omega_n}\arccos\left(\dfrac{\omega_n^2 - d_1d_2\lambda_n^2 + d_2\lambda_na_1}{(\chi\alpha\lambda_n - a_2)b}\right), \quad 1 \leq n \leq N, \end{cases} \tag{3.16}$$

where N is defined in Lemma 3.1. Then, we have the following statements:

(i) τ_{00} is constant with respect to χ, $\tau_{n0}(\chi)$ monotonically decreases with respect to χ for $1 \leq n \leq N$, and

$$\lim_{\chi \to \infty} \tau_{n0}(\chi) = 0;$$

(ii) When $\chi = 0$, $\tau_{n0}(0)$ is a monotonically increasing function with respect to n for $0 \leq n \leq N$, that is,

$$\tau_{00} = \min_{0 \leq n \leq N} \tau_{n0}(0).$$

Proof. (i) τ_{00} is constant for χ. Next, we will demonstrate that $\tau_{n0}(\chi)$ is a strictly decreasing function with respect to χ for $1 \le n \le N$. Additionally, ω_n is a function of χ, satisfying Eq (3.8). First, differentiating both sides of Eq (3.8) with respect to χ, we obtain

$$4\omega_n^3\frac{d\omega_n(\chi)}{d\chi} + 2\omega_n\frac{d\omega_n(\chi)}{d\chi}[(d_1\lambda_n - a_1)^2 + d_2^2\lambda_n^2] - 2b^2(\chi\alpha\lambda_n - a_2)\alpha\lambda_n = 0.$$

Then,

$$\frac{d\omega_n(\chi)}{d\chi} = \omega_n'(\chi) = \frac{2b^2\alpha\lambda_n(\chi\alpha\lambda_n - a_2)}{4\omega_n^3(\chi) + 2[(d_1\lambda_n - a_1)^2 + d_2^2\lambda_n^2]\omega_n} > 0. \tag{3.17}$$

Taking the derivative on both sides of the second equation in (3.16) with respect to χ, we obtain

$$\frac{d(\tau_{n0}(\chi))}{d\chi} = -\frac{\omega_n'(\chi)}{\omega_n^2(\chi)}\arccos H_n - \frac{1}{\omega_n(\chi)\sqrt{1 - H_n^2}}H_n'(\chi),$$

where

$$H_n(\chi) = \frac{\omega_n^2 - d_1d_2\lambda_n^2 + d_2\lambda_n a_1}{(\chi\alpha\lambda_n - a_2)b},$$

and $\omega_n'(\chi)$ is defined in (3.17). Next, differentiating $H_n(\chi)$ with respect to χ, we get

$$H_n'(\chi) = \frac{2\omega_n(\chi)\omega_n'(\chi)(\chi\alpha\lambda_n - a_2)b - (\omega_n^2(\chi) - d_1d_2\lambda_n^2 + d_2\lambda_n a_1)\alpha\lambda_n}{(\chi\alpha\lambda_n - a_2)^2 b}.$$

Since $0 < \arccos H_n < \pi$ and $\omega_n'(\chi) > 0$, it follows that $\frac{d(\tau_{n0}(\chi))}{d\chi} < 0$. Thus, $\tau_{n0}(\chi)$ is a monotonically decreasing function with respect to χ for $0 \le n \le N$. Based on Eq (3.17), $\omega_n(\chi) \to +\infty$ when $\chi \to +\infty$, that is $\lim\limits_{\chi\to+\infty}\frac{1}{\omega_n(\chi)} = 0$. Moreover, $\arccos H_n$ is a bounded function, so $\lim\limits_{\chi\to+\infty}\tau_{n0}(\chi) = 0$.

(ii) When $\chi = 0$, let $\lambda_n = p$, and the second equation in (3.16) can be rewritten as

$$\tau_{n0}(0) = \tau_{p0}(0) = \frac{1}{\omega_n(0)}\arccos\frac{\omega_n^2(0) - d_1d_2p^2 + d_2pa_1}{-a_2b},\ 0 \le n \le N. \tag{3.18}$$

Denote $\omega_n(0) = \widetilde{\omega}_n(p)$, where $\widetilde{\omega}_n(p)$ satisfies

$$\widetilde{\omega}_n^4(p) + [(d_1p - a_1)^2 + d_2^2p^2]\widetilde{\omega}_n^2(p) + (d_1d_2p^2 - d_2pa_1)^2 + a_2^2b^2 = 0. \tag{3.19}$$

Differentiating both sides of Eq (3.19) with respect to p, we obtain

$$\widetilde{\omega}_n'(p) = -\frac{\widetilde{\omega}_n^2(p)[2d_1(d_1p - a_1) + 2d_2^2p] + 2(d_1d_2p^2 - a_1d_2p)(2d_1d_2p - d_2a_1)}{4\widetilde{\omega}_n^3(p) + 2[(d_1p - a_1)^2 + d_2^2p^2]\widetilde{\omega}_n(p)} < 0.$$

Then, taking the derivative of Eq (3.18) with respect to p, we have

$$\frac{d(\tau_{p0}(0))}{dp} = -\frac{\widetilde{\omega}_n'(p)}{\widetilde{\omega}_n^2(p)}\arccos\widetilde{H}_n - \frac{1}{\widetilde{\omega}_n(p)\sqrt{1 - \widetilde{H}_n^2}}\widetilde{H}_n'.$$

Since $\widetilde{H}_n = H_n|_{\chi=0}$, $\widetilde{\omega}_n'(p) < 0$, and $a_2 < 0$, we get $\frac{d(\tau_{p0}(0))}{dp} > 0$. This means τ_{p0} is monotonically increasing with respect to p. However, p is proportional to n, then τ_{n0} increases monotonically with respect to n, that is $\tau_{00}(0) < \tau_{10}(0) < \cdots < \tau_{N0}(0)$. This completes the proof. □

Using Lemmas 3.1 and 3.2, we obtain the stability of the coexistence equilibrium and the properties of the Hopf bifurcation in system (1.2) as follows.

Theorem 3.1. *Define* $\chi^* = \min\limits_{1\le n\le N}\chi_n$, *where* χ_n *is a solution of the equation* $\tau_{00} = \tau_{n0}(\chi)$.
(*i*) ***(Bifurcation)*** χ_* *is defined by Eq* (3.11). *Then, we have the following results:*

(*a*) *If* $0 < \chi \le \chi_*$, *system* (1.2) *undergoes spatially homogeneous Hopf bifurcations at* $\tau = \tau_{0j}$ *for* $j \in \mathbb{N}_0$, *where* $\tau_{00} = \min\limits_{j\in\mathbb{N}_0}\tau_{0j}$ *is the critical value for the Hopf bifurcation, and the first Hopf bifurcation is spatially homogeneous.*

(*b*) *If* $\chi_* < \chi \le \chi^*$, *system* (1.2) *undergoes mode-n Hopf bifurcations at* $\tau = \tau_{nj}$ *for* $0 \le n \le N$ *and* $j \in \mathbb{N}_0$, *where* $\tau_{00} = \min\limits_{0\le n\le N}\tau_{n0}$ *is the critical value for Hopf bifurcation, so the first Hopf bifurcation is spatially homogeneous.*

(*c*) *If* $\chi > \chi^*$, *system* (1.2) *undergoes mode-n Hopf bifurcation at* $\tau = \tau_{nj}$ *for* $0 \le n \le N$ *and* $j \in \mathbb{N}_0$. *Since there is no absolute order for* τ_{n0}, *thus we define* $\tau_* = \min\limits_{1\le n\le N}\tau_{n0}$ *as the first critical value for the Hopf bifurcation, at which the periodic solutions are spatially nonhomogeneous.*

(*d*) *If* $\chi > \chi_*$, *there exists double Hopf bifurcation due to the interaction between homogeneous and nonhomogeneous or between nonhomogeneous Hopf bifurcations with different modes.*
(*ii*) ***(Stability)*** *The stability analysis of coexistence equilibrium* E_* *is as follows:*

(*a*) *If* $0 < \chi \le \chi^*$, *the positive equilibrium* (u_*, v_*) *of system* (1.2) *is locally asymptotically stable for* $\tau \in [0, \tau_{00})$ *and unstable for* $\tau \in (\tau_{00}, +\infty)$. *Then the periodic solution bifurcating from* $\tau = \tau_{00}$ *is spatially homogeneous.*

(*b*) *If* $\chi > \chi^*$, *the positive equilibrium* (u_*, v_*) *is local asymptotically stable with respect to* $\tau \in [0, \tau_*)$ *and unstable with respect to* $\tau \in (\tau_*, +\infty)$, *and the periodic solution bifurcating from* $\tau = \tau_*$ *is spatially nonhomogeneous.*

Proof. (i)-(a). When $0 < \chi \le \chi_*$, rewriting the characteristic Eq (3.4), we have

$$\mu^2 + A_k\mu + B_k + C_k b e^{-\mu\tau} = 0, \tag{3.20}$$

where $A_k = d_1\lambda_n + d_2\lambda_n - a_1$, $B_k = d_1d_2\lambda_n^2 - d_2\lambda_n a_1$, and $C_k = \chi\alpha\lambda_n - a_2$.

To verify the transversality conditions, we take the derivative of Eq (3.20) with respect to τ, getting

$$2\mu\frac{d\mu}{d\tau} + A_k\frac{d\mu}{d\tau} + C_k b e^{-\mu\tau}\left(-\mu - \tau\frac{d\mu}{d\tau}\right) = 0,$$

then

$$\left(\frac{d\mu}{d\tau}\right)^{-1} = \frac{2\mu + A_k - C_k b\tau e^{-\mu\tau}}{C_k b\mu e^{-\mu\tau}} = \frac{2\mu + A_k}{C_k b\mu e^{-\mu\tau}} - \frac{\tau}{\mu}. \tag{3.21}$$

Using Eqs (3.7) and (3.21), we obtain

$$\begin{aligned} sign\left[\mathrm{Re}\left(\frac{d\mu}{d\tau}\right)^{-1}\right]_{\tau=\tau_{nj}} &= sign\mathrm{Re}\left[\frac{2\mu+A_k}{C_k b\mu e^{-\mu\tau}} - \frac{\tau}{\mu}\right]_{\tau=\tau_{nj}} = sign\mathrm{Re}\left[\frac{2i\omega_n + A_k}{C_k bi\omega_n[\cos(\omega_n\tau_{nj}) - i\sin(\omega_n\tau_{nj})]}\right] \\ &= sign\left[\frac{2\omega_n^2 - 2(d_1d_2\lambda_n^2 - d_2\lambda_n a_1) + (d_1\lambda_n + d_2\lambda_n - a_1)^2}{C_k^2 b^2}\right] = sign\left[\frac{2\omega_n^2 - 2B_k + A_k^2}{C_k^2 b^2}\right]. \end{aligned}$$

Since $A_k^2 - 2B_k > 0$, we have $sign\left[\mathrm{Re}\left(\frac{d\mu}{d\tau}\right)^{-1}\right]_{\tau=\tau_{nj}} > 0$, that is, $sign\left[\mathrm{Re}\left(\frac{d\mu}{d\tau}\right)\right]_{\tau=\tau_{nj}} > 0$. Thus, the Hopf bifurcation at $\tau = \tau_{nj}$ indeed occurs, where $\tau_{n0} = \min\limits_{j\in\mathbb{N}_0} \tau_{nj}$. Thus, (i)-(a) holds.

(i)-(b). When $\chi_* < \chi \leq \chi^*$, $\tau_{n0}(\chi)$ is a monotonically decreasing function with respect to χ, and τ_{00} is constant with respect to χ. There exists $\tau_{00} < \tau_{n0}$ when $\chi = 0$ and $\tau_{n0} \to 0$ when $\chi \to +\infty$. This implies that there exists χ_n such that τ_{00} and τ_{n0} intersect at $\chi = \chi_n$, where $n = 1, 2, \cdots, N$, and $\chi^* = \min\limits_{1\leq n\leq N} \chi_n$. Furthermore, because $\tau_{00} = \min\limits_{0\leq n\leq N} \tau_{n0}$ is the first critical point for the occurrence of a Hopf bifurcation, the periodic solution at the first critical value is spatially homogeneous. Thus, (i)-(b) holds.

(i)-(c). When $\chi > \chi^*$, according to Lemma 3.1, Hopf bifurcations are possible for wave number $0 \leq n \leq N$. Moreover, the first critical value of the Hopf bifurcation depends on χ rather than τ_{00}, so we define the first critical value as $\tau_* = \min\limits_{1\leq n\leq N} \tau_{n0}$. Consequently, the Hopf bifurcation at the first critical point leads to spatially nonhomogeneous periodic solutions. Thus, (i)-(c) holds.

(i)-(d). When $\chi > \chi_*$, the critical values $\tau_{n0}(\chi)$ for $1 \leq n \leq N$ are strictly monotonically decreasing with respect to χ, while τ_{00} is constant with respect to χ. Obviously, $\lim\limits_{\chi\to+\infty} \tau_{n0}(\chi) = 0$, and $\tau_{00} < \tau_{n0}(0)$ when $\chi = 0$. For different $1 \leq n \leq N$, the bifurcation curve $\tau = \tau_{n0}(\chi)$ exists intersection points and bifurcations occur at these points. The double Hopf bifurcations emerge by the interaction between homogeneous and nonhomogeneous or between nonhomogeneous Hopf bifurcations with different modes. Thus, (i)-(d) holds.

(ii)-(a). According to conclusion (*i*), the first critical value of Hopf bifurcation is attained at τ_{00} when $0 < \chi \leq \chi^*$. Using Hopf bifurcation theory, the equilibrium E_* is locally asymptotically stable for $\tau \in [0, \tau_{00})$ and unstable for $\tau \in (\tau_{00}, +\infty)$, and the periodic solution is homogeneous in space. Thus, (ii)-(a) holds.

(ii)-(b). According to conclusion (*i*), the first critical value of Hopf bifurcation is attained at $\tau_* = \min\limits_{1\leq n\leq N} \tau_{n0}$ when $\chi > \chi^*$. Using Hopf bifurcation theory, the equilibrium E_* is locally asymptotically stable for $\tau \in [0, \tau_*)$ and unstable for $\tau \in (\tau_*, +\infty)$, with the periodic solution being spatially nonhomogeneous. Thus, (ii)-(b) holds. □

Remark 3.1. (*i*) *From Theorem 3.1, it is evident that χ^* affects the occurrence of spatially nonhomogeneous Hopf bifurcations.*

(*ii*) *According to the definition of χ_* in* (3.11)*, there exists a spatial critical value l_0 such that: (a) when $0 < l < l_0$, a spatially nonhomogeneous Hopf bifurcation does not occur for $0 < \chi \leq \chi^*$; (b) when $l > l_0$, a spatially nonhomogeneous Hopf bifurcations occur for $\chi > 0$ due to the critical value $\chi^* = 0$.*

4. Turing-Hopf bifurcation

Next, we will consider the occurrence of a Turing-Hopf bifurcation in system (1.2). We rewrite the linearized system (3.1) as follows:

$$\begin{cases} \dfrac{\partial u}{\partial t} = d_1\Delta u + \chi\alpha\Delta v - \dfrac{r\alpha}{K}u - \dfrac{a\alpha}{(1+hv_*)^2}v, & x \in \Omega,\ t > 0, \\ \dfrac{\partial v}{\partial t} = d_2\Delta v + \dfrac{sv_*^2}{(\alpha+e)^2}u(x, t-\tau), & x \in \Omega,\ t > 0, \\ \dfrac{\partial u}{\partial \mathbf{n}} = \dfrac{\partial v}{\partial \mathbf{n}} = 0, & x \in \partial\Omega,\ t > 0, \\ u(x,0) = u(x) > 0, v(x,0) = v(x) > 0, & x \in \Omega. \end{cases} \tag{4.1}$$

Setting

$$u(x, t-\tau) = u(x,t) - \tau\frac{\partial u(x,t)}{\partial t},$$

and putting it into (4.1), we get

$$\begin{cases} \dfrac{\partial u}{\partial t} = d_1\Delta u + \chi\alpha\Delta v - \dfrac{r\alpha}{K}u - \dfrac{a\alpha}{(1+hv_*)^2}v, & x \in \Omega,\ t > 0, \\ \dfrac{sv_*^2}{(\alpha+e)^2}\tau\dfrac{\partial u}{\partial t} + \dfrac{\partial v}{\partial t} = d_2\Delta v + \dfrac{sv_*^2}{(\alpha+e)^2}u, & x \in \Omega,\ t > 0, \\ \dfrac{\partial u}{\partial \mathbf{n}} = \dfrac{\partial v}{\partial \mathbf{n}} = 0, & x \in \partial\Omega,\ t > 0, \\ u(x,0) = u(x) > 0, v(x,0) = v(x) > 0, & x \in \Omega. \end{cases} \tag{4.2}$$

That is,

$$B_\tau \begin{pmatrix} \frac{\partial u}{\partial t} \\ \frac{\partial v}{\partial t} \end{pmatrix} = D\begin{pmatrix} u \\ v \end{pmatrix} + J_0\begin{pmatrix} u \\ v \end{pmatrix}, \tag{4.3}$$

where

$$B_\tau = \begin{pmatrix} 1 & 0 \\ \frac{sv_*^2}{(\alpha+e)^2}\tau & 1 \end{pmatrix},\ D = \begin{pmatrix} d_1\Delta & \chi\alpha\Delta \\ 0 & d_2\Delta \end{pmatrix},\ J_0 = \begin{pmatrix} -\frac{r\alpha}{K} & -\frac{a\alpha}{(1+hv_*)^2} \\ \frac{sv_*^2}{(\alpha+e)^2} & 0 \end{pmatrix}.$$

Consider the following general solution of (4.3)

$$\begin{pmatrix} u \\ v \end{pmatrix} = \sum_{k=0}^{\infty}\begin{pmatrix} a_k \\ b_k \end{pmatrix}e^{\lambda_k t}\cos kx,$$

where a_k and b_k are constants, k is the spatial spectrum, and λ_k means the temporal spectrum. Then, putting it into (4.3), one gets

$$\lambda_k\begin{pmatrix} 1 & 0 \\ \frac{sv_*^2}{(\alpha+e)^2}\tau & 1 \end{pmatrix}\sum_{k=0}^{\infty}\begin{pmatrix} a_k \\ b_k \end{pmatrix}e^{\lambda_k t}\cos kx = \begin{pmatrix} -d_1k^2 - \frac{r\alpha}{K} & -\chi\alpha k^2 - \frac{a\alpha}{(1+hv_*)^2} \\ \frac{sv_*^2}{(\alpha+e)^2} & -d_2k^2 \end{pmatrix}\sum_{k=0}^{\infty}\begin{pmatrix} a_k \\ b_k \end{pmatrix}e^{\lambda_k t}\cos kx.$$

That is,

$$\begin{vmatrix} \lambda_k + d_1k^2 + \frac{r\alpha}{K} & \chi\alpha k^2 + \frac{a\alpha}{(1+hv_*)^2} \\ \frac{sv_*^2}{(\alpha+e)^2}(\tau\lambda_k - 1) & \lambda_k + d_2k^2 \end{vmatrix} = 0.$$

We obtain the characteristic equation as follows:

$$\lambda_k^2 - T_k(\tau,\chi)\lambda_k + D_k(\tau,\chi) = 0, \quad k \in \mathbb{N}_0 = \{0, 1, 2, 3, ...\}, \tag{4.4}$$

where

$$T_k(\tau,\chi) = -\left(d_1k^2 + d_2k^2 + \frac{r\alpha}{K}\right) + \left(\chi\alpha k^2 + \frac{a\alpha}{(1+hv_*)^2}\right).\frac{sv_*^2\tau}{(\alpha+e)^2},$$

and

$$D_k(\tau,\chi) = d_2k^2\left(d_1k^2 + \frac{r\alpha}{K}\right) + \left(\chi\alpha k^2 + \frac{a\alpha}{(1+hv_*)^2}\right).\frac{sv_*^2}{(\alpha+e)^2}.$$

Thus, we have

$$\lambda_0^2 - T_0(\tau,\chi)\lambda_0 + D_0(\tau,\chi) = 0, \tag{4.5}$$

where

$$T_0(\tau,\chi) = -\frac{r\alpha}{K} + \frac{a\alpha}{(1+hv_*)^2}\cdot\frac{sv_*^2\tau}{(\alpha+e)^2},\ D_0(\tau,\chi) = \frac{a\alpha}{(1+hv_*)^2}\cdot\frac{sv_*^2}{(\alpha+e)^2} > 0.$$

For the spatially homogeneous system, setting $T_0(\tau,\chi) = 0$, one gets

$$\tau_c = \frac{r}{K}\cdot\frac{(1+hv_*)^2}{a}\frac{(\alpha+e)^2}{sv_*^2}.$$

So $T_0(\tau,\chi) < 0$ when $0 < \tau < \tau_c$. All eigenvalues of the characteristic Eq (4.5) have negative real parts, which means that the positive equilibrium E_* is locally asymptotically stable. And E_* is unstable when $\tau > \tau_c$. Due to

$$\left.\frac{d\mathrm{Re}(\lambda_0)}{d\tau}\right|_{\tau=\tau_c} = \frac{a\alpha}{(1+hv_*)^2}\cdot\frac{sv_*^2}{(\alpha+e)^2} > 0.$$

For the homogeneous system, the Hopf bifurcation will occur when $\tau = \tau_c$. And $T_0(\tau,\chi) < 0$ and $D_0(\tau,\chi) > 0$ when $\tau = 0$, and the positive equilibrium E_* is locally asymptotically stable. Thus, the Turing-Hopf bifurcation does not occur if there is no digestion delay in system (4.2).

Next, let $d_1, d_2 \neq 0$, $\chi \neq 0$, and $0 < \tau < \tau_c$ to further investigate the Turing instability. We rewrite $T_k(\tau,\chi)$ as

$$T_k(\tau,\chi) = -\left(-\frac{sv_*^2\tau\chi\alpha}{(\alpha+e)^2} + d_1 + d_2\right)k^2 + T_0(\tau,\chi).$$

Clearly, $T_k(\tau,\chi) < 0$ when $-\frac{sv_*^2\tau\chi\alpha}{(\alpha+e)^2} + d_1 + d_2 > 0$. That is,

$$\chi < \frac{(d_1+d_2)(\alpha+e)^2}{sv_*^2\tau\alpha} = \chi_0.$$

Thus, we only consider the sign of $D_k(\tau,\chi)$. Set $D_k(\tau,\chi)\hat{=}\varphi(k^2)$, where

$$\varphi(k^2) = d_1d_2k^4 + \left(\frac{rd_2\alpha}{K} + \frac{sv_*^2\chi\alpha}{(\alpha+e)^2}\right)k^2 + \frac{a\alpha}{(1+hv_*)^2}.\frac{sv_*^2}{(\alpha+e)^2}.$$

Due to $\varphi(0) = \frac{a\alpha}{(1+hv_*)^2}.\frac{sv_*^2}{(\alpha+e)^2} > 0$, let $k^2 = p$, and one gets

$$\varphi(p) = d_1d_2p^2 + \left(\frac{rd_2\alpha}{K} + \frac{sv_*^2\chi\alpha}{(\alpha+e)^2}\right)p + \frac{a\alpha}{(1+hv_*)^2}.\frac{sv_*^2}{(\alpha+e)^2},\ p \in [0,+\infty).$$

Considering $\min\limits_{p>0}\varphi(p) = 0$, by differentiating with respect to $\varphi(p) = 0$, we obtain

$$p_0 = \frac{\frac{rd_2\alpha}{K} + \frac{sv_*^2\chi\alpha}{(\alpha+e)^2}}{2d_1d_2}.$$

So, $\min\limits_{p>0} \varphi(p) = -\phi(\chi) = 0$, where

$$\phi(\chi) = \alpha^2\left(\frac{sv_*^2}{(\alpha+e)^2}\right)^2\chi^2 + \frac{2d_2r\alpha^2}{K}\cdot\frac{sv_*^2}{(\alpha+e)^2}\chi + \frac{d_2^2r^2\alpha^2}{K^2} - \frac{4d_1d_2a\alpha}{(1+hv_*)^2}\cdot\frac{sv_*^2}{(\alpha+e)^2}.$$

For $\frac{16d_1d_2ab^3\alpha^3}{(1+hv_*)^2} > 0$, it implies that $\phi(\chi) = 0$ has two different roots.

Case I. $\frac{d_2^2r^2\alpha^2}{K^2} - \frac{4d_1d_2a\alpha}{(1+hv_*)^2}\cdot\frac{sv_*^2}{(\alpha+e)^2} > 0:$ $\phi(\chi) = 0$ must have two negative roots $\chi_1 < 0$ and $\chi_2 < 0$, where

$$\chi_1 = \frac{-\frac{d_2r\alpha}{K} - \frac{2}{1+hv_*}\cdot\sqrt{d_1d_2a\alpha\cdot\frac{sv_*^2}{(\alpha+e)^2}}}{\alpha\cdot\frac{sv_*^2}{(\alpha+e)^2}} < 0,$$

$$\chi_2 = \frac{-\frac{d_2r\alpha}{K} + \frac{2}{1+hv_*}\cdot\sqrt{d_1d_2a\alpha\cdot\frac{sv_*^2}{(\alpha+e)^2}}}{\alpha\cdot\frac{sv_*^2}{(\alpha+e)^2}} < 0.$$

It is clear that $\phi(\chi) > 0$ if $\chi < \chi_1$ and $\chi > \chi_2$, and $\phi(\chi) < 0$ if $\chi_1 < \chi < \chi_2$. Then we get $\varphi(k^2) > 0$ if $\chi_1 < \chi < \chi_2$, and $\varphi(k^2) < 0$ if $\chi < \chi_1$ and $\chi > \chi_2$ for some $k \in \mathbb{N}_0/\{0\}$. Recalling the definition of χ_0, we have the following results. If $\chi_1 < \chi < \min\{\chi_0, \chi_2\}$, the positive equilibrium E_* is locally asymptotically stable and no Turing bifurcation will appear in system (4.2). If $\chi < \min\{\chi_0, \chi_1\}$ or $\chi_2 < \chi < \chi_0$, the positive equilibrium E_* is unstable, and the Turing bifurcation will occur in system (4.2).

Case II. $\frac{d_2^2r^2\alpha^2}{K^2} - \frac{4d_1d_2a\alpha}{(1+hv_*)^2}\cdot\frac{sv_*^2}{(\alpha+e)^2} < 0:$ $\phi(\chi) = 0$ must have two roots $\chi_3 < 0$ and $\chi_4 \geq 0$, where

$$\chi_3 = \frac{-\frac{d_2r\alpha}{K} - \frac{2}{1+hv_*}\cdot\sqrt{d_1d_2a\alpha\cdot\frac{sv_*^2}{(\alpha+e)^2}}}{\alpha\cdot\frac{sv_*^2}{(\alpha+e)^2}} < 0,$$

$$\chi_4 = \frac{-\frac{d_2r\alpha}{K} + \frac{2}{1+hv_*}\cdot\sqrt{d_1d_2a\alpha\cdot\frac{sv_*^2}{(\alpha+e)^2}}}{\alpha\cdot\frac{sv_*^2}{(\alpha+e)^2}} \geq 0.$$

It is clear that $\phi(\chi) > 0$ if $\chi < \chi_3$ and $\chi > \chi_4$, and $\phi(\chi) < 0$ if $\chi_3 < \chi < \chi_4$. Then, we get $\varphi(k^2) > 0$ if $\chi_3 < \chi < \chi_4$, and $\varphi(k^2) < 0$ if $\chi < \chi_3$ and $\chi > \chi_4$ for some $k \in \mathbb{N}_0/\{0\}$. Hence, if $\chi_3 < \chi < \min\{\chi_0, \chi_4\}$, the positive equilibrium E_* is locally asymptotically stable, and no Turing instability will appear in system (4.2). If $\chi < \min\{\chi_0, \chi_3\}$ or $\chi_4 < \chi < \chi_0$, the positive equilibrium E_* is unstable, and a Turing instability will occur in system (4.2).

Theorem 4.1. ***(Turing-Hopf bifurcation)***

For $d_1, d_2 > 0$, system (1.2) *will undergo a Turing-Hopf bifurcation when $\tau = \tau_c$ and $\chi = \chi_{c1}$ or $\chi = \chi_{c2}$, where*

$$\tau_c = -\frac{r}{K}\cdot\frac{(1+hv_*)^2}{a}\frac{(\alpha+e)^2}{sv_*^2},$$

$$\chi_{c1} = \frac{-\frac{d_2 r\alpha}{K} - \frac{2}{1+hv_*} \cdot \sqrt{d_1 d_2 a\alpha \cdot \frac{sv_*^2}{(\alpha+e)^2}}}{\alpha \cdot \frac{sv_*^2}{(\alpha+e)^2}}, \chi_{c2} = \frac{-\frac{d_2 r\alpha}{K} + \frac{2}{1+hv_*} \cdot \sqrt{d_1 d_2 a\alpha \cdot \frac{sv_*^2}{(\alpha+e)^2}}}{\alpha \cdot \frac{sv_*^2}{(\alpha+e)^2}}.$$

5. Numerical simulations

In this section, numerical simulations are carried out to verify theoretical analysis results. We consider system (1.2) in a fixed domain $\Omega = (0, L)$ and solve it on a grid with $1 \times N$ sites. By using finite difference, we discretize the Laplacian in the grid with lattice sites denoted by i. We denote $\Delta x = L/N$, where N is the number of discrete points. The form is $\Delta w|_i = (w_{i+1} - 2w_i + w_{i-1})/\Delta x^2$, $1 \le i \le N$. Then, we employ the explicit Euler method, and the time step is $\Delta t = 0.001$. The initial values are taken as $(u_0, v_0) = (u_* - 0.02\cos(x), v_* - 0.02\cos(x))$.

First, we choose the parameters (i) $d_1 = 0.1$, $d_2 = 0.1$, $s = 16$, $e = 1$, $d = 13$, $h = 4$, $r = 2$, $K = 1$, and $a = 10$, and one obtains the unique positive equilibrium $(u_*, v_*) = (0.2308, 0.4)$, $a_1 = -0.4615$, $a_2 = -0.3414$, $b = 1.69$, and $l_0 = 0.2431$. According to the definition of χ_*, we choose $l = 0.2 < l_0$ and $l = 2 > l_0$, respectively. χ_*=0.7002 when $l = 0.2$, and χ_*=0 when $l = 2$. The bifurcation diagrams in the $\chi - \tau$ plane are shown in Figure 1.

From Figure 1(a), we find that the critical value of the spatially nonhomogeneous Hopf bifurcation is $\chi_* = 0.7002$. Figure 1(b) indicates that a spatially nonhomogeneous Hopf bifurcation will emerge for $\chi_* > 0$. Moreover, when $\chi < \chi^* = 0.686$, the critical value for the Hopf bifurcation is $\tau_{00} = 0.848$, and when $\chi > \chi^* = 0.686$, the critical value for the Hopf bifurcation is $\tau_* = \min_{0 \le n \le 4} \tau_{n0}$. The blue region in Figure 1(b) represents the stable region corresponding to $\tau < \tau_{00}$ and $\tau < \tau_*$, while the regions corresponding to $\tau > \tau_{00}$ or $\tau > \tau_*$ denote the unstable regions. Additionally, we note that the intersection points of adjacent curves (such as mode-1 and mode-2) are double Hopf bifurcation points. Next, we further select different digestion delay τ and predator-taxis sensitivity parameter χ to conduct numerical simulations.

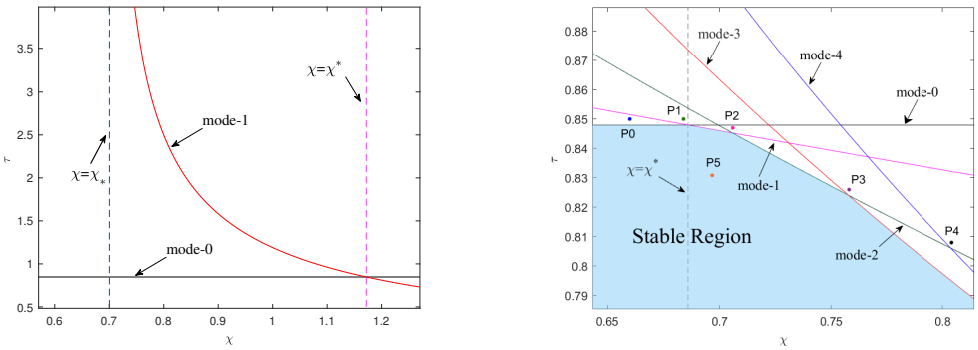

(a) (b)

Figure 1. The bifurcation diagrams of system (1.2) in the $\chi - \tau$ plane. (a) The bifurcation diagram when $l = 0.2 < l_0$. mode$-k, k = 0, 1$ are Hopf bifurcation curves. (b) The stability regions and bifurcation diagram when $l = 2 > l_0$. mode$-k, k = 0, 1, \cdots, 4$ are Hopf bifurcation curves, and the blue region represents the stable region. P0(0.66,0.85), P1(0.69,0.85), P2(0.706,0.847), P3(0.758,0.826), P4(0.804,0.808), and P5(0.696,0.831) are chosen for numerical simulations.

Figure 2 illustrates spatiotemporal patterns of prey for mode$-k, k = 0, 1, \cdots, 4$, where Figure 2(a) represents spatially homogeneous periodic patterns, Figure 2(b)–(e) show spatiotemporal nonhomogeneous periodic patterns for mode $-k, k = 1, \cdots, 4$, and Figure 2(f) shows the coexistence equilibrium (u_*, v_*) is asymptotically stable for (χ, τ) at P5(0.696,0.831). Subsequently, the spatially nonhomogeneous periodic patterns with different modes are shown in Figure 3.

It is found that the interaction of the spatially nonhomogeneous Hopf bifurcation leads to a more complex phenomenon which is known as the double Hopf bifurcation. The transition of prey and predator from the spatially nonhomogeneous periodic solution of mode-3 and mode-4 can be clearly observed, see Figures 3(d) and 4. And, Figures 4(b) and (d) further show that spatially nonhomogeneous periodic solutions are unstable during the transition of patterns. Also, Figure 5 illustrates the dynamic curves of periodic solutions of predator and prey at spatial positions $x = 2\pi$ and $x = \pi$ in the temporal direction, respectively. It can be observed that population density exhibits periodicity in time and a nonhomogeneous distribution in space.

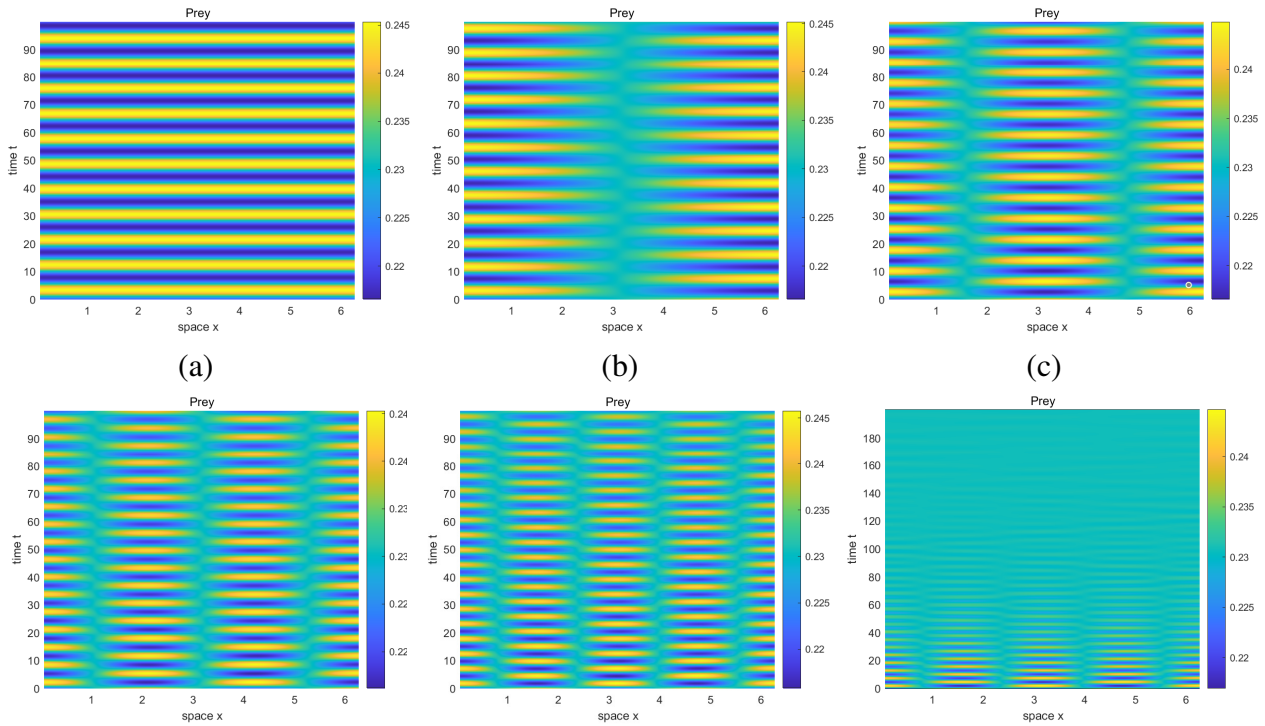

Figure 2. The spatiotemporal patterns of the density of prey population in system (1.2) for P0(0.66,0.85), P1(0.69,0.85), P2(0.706,0.847), P3(0.758,0.826), P4(0.804,0.808), and P5(0.696,0.831), respectively. (a) The stable spatially homogeneous periodic pattern for mode-0. (b)–(e) The spatially nonhomogeneous periodic patterns for mode$-k, k = 1, \cdots, 4$ with $l = 2$. (f) The positive equilibrium is asymptotically stable at P5(0.696,0.831).

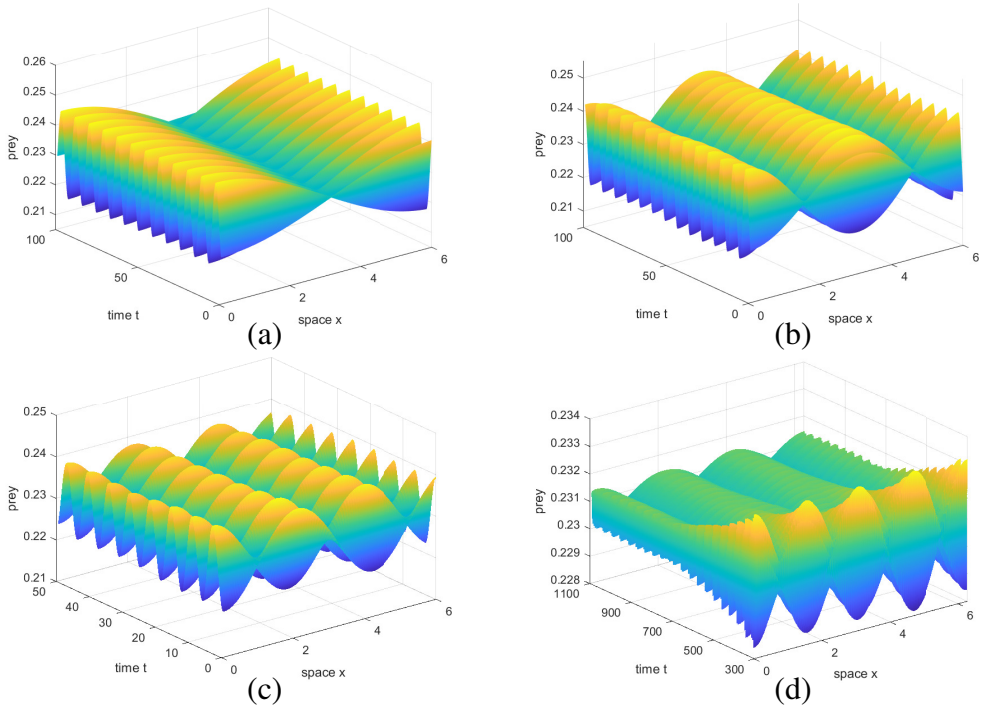

Figure 3. The nonhomogeneous periodic patterns of system (1.2) about prey for mode $-k, k$=1, $\cdots$, 4 with $l = 2$.

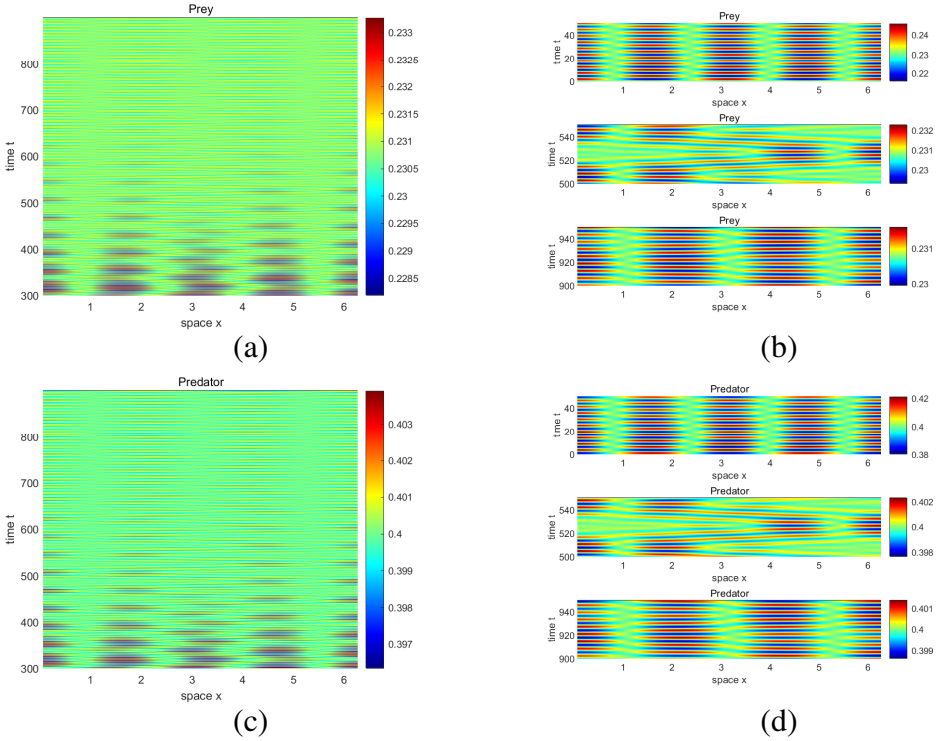

Figure 4. The spatiotemporal dynamics of system (1.2) with $l = 2$ and P4(0.804,0.808). (a) and (c): The spatiotemporal dynamics of system (1.2) for prey and predator, respectively. (b) and (d): The transition from the spatially nonhomogeneous periodic solution of mode-4 to mode-3.

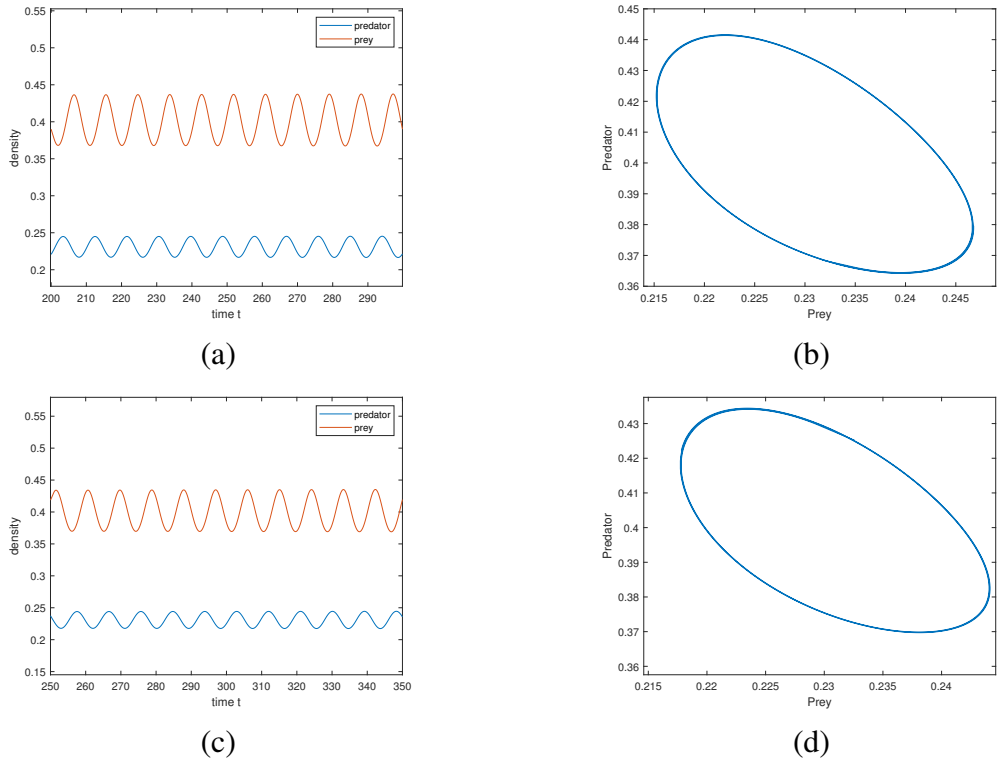

Figure 5. The bifurcation periodic solutions of prey and predator, $\tau = 0.85, \chi = 0.76$. (a) and (b) are the dynamic curve of the periodic solution and the phase diagram with $x = 2\pi$. (c) and (d) are the dynamic curve of the periodic solution and the phase diagram with $x = \pi$.

Next, we choose the parameters (ii) $d_1 = 0.2$, $d_2 = 2$, $s = 16$, $e = 1$, $d = 13$, $h = 4$, $r = 2$, $K = 1$, $a = 10$, one obtains $E_* = (0.2308, 0.4)$, $\tau_c = 0.8$, $\frac{d_2^2 r^2 \alpha^2}{K^2} - \frac{4d_1 d_2 a\alpha}{(1+hv_*)^2} \cdot \frac{sv_*^2}{(\alpha+e)^2} = -0.071 < 0$, $\chi_0 = 8.0586$, $\chi_{c1} = -4.8304$, and $\chi_{c2} = 0.0966$. When $\chi = -5.5 < \min\{-4.8304, 8.0586\}$ and $\tau = 0.7 < 0.8$, the Turing bifurcation emerges. It is shown that the spatially nonhomogeneous steady patterns occur in system (1.2), see Figure 6.

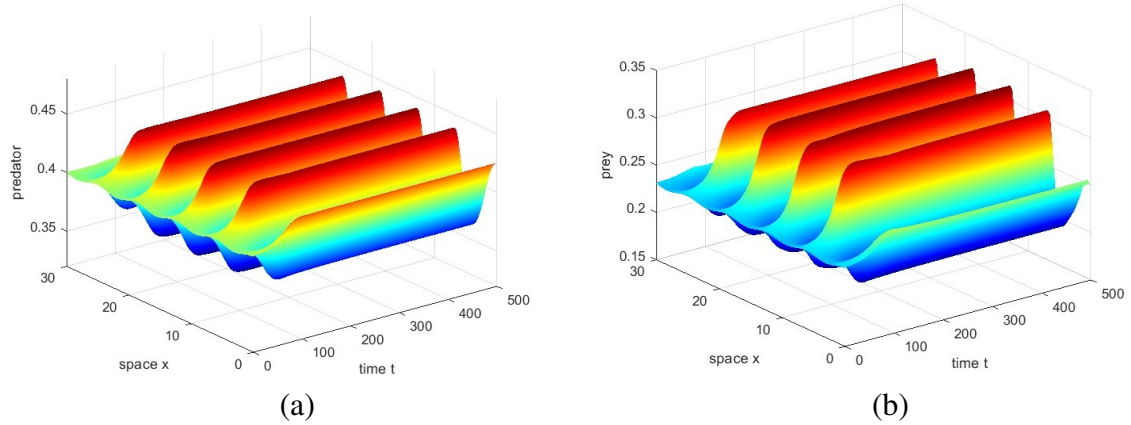

Figure 6. The spatially nonhomogeneous steady patterns induced by the Turing bifurcation in system (1.2).

Similarly, we choose the parameters (iii) $d_1 = 0.2$, $d_2 = 3$, $s = 1.5$, $e = 0.8$, $d = 1$, $h = 0.5$, $r = 1$, $K = 1.5$, $a = 1$. Then, one obtains $E_* = (0.7, 0.7273)$, $\tau_c = 3.5156$, $\frac{d_2^2 r^2 \alpha^2}{K^2} - \frac{4d_1 d_2 a\alpha}{(1+hv_*)^2} \cdot \frac{sv_*^2}{(\alpha+e)^2} = 1.6414 > 0$, $\chi_0 = 4.3214$, $\chi_{c1} = -7.9586$, and $\chi_{c2} = -3.3852$. When $\chi = -10 < \min\{-7.9586, 4.3214\}$ and $\tau = 3 < 3.5156$, the Turing bifurcation emerges. It is shown that the spatially nonhomogeneous steady patterns occur in system (1.2), see Figure 7.

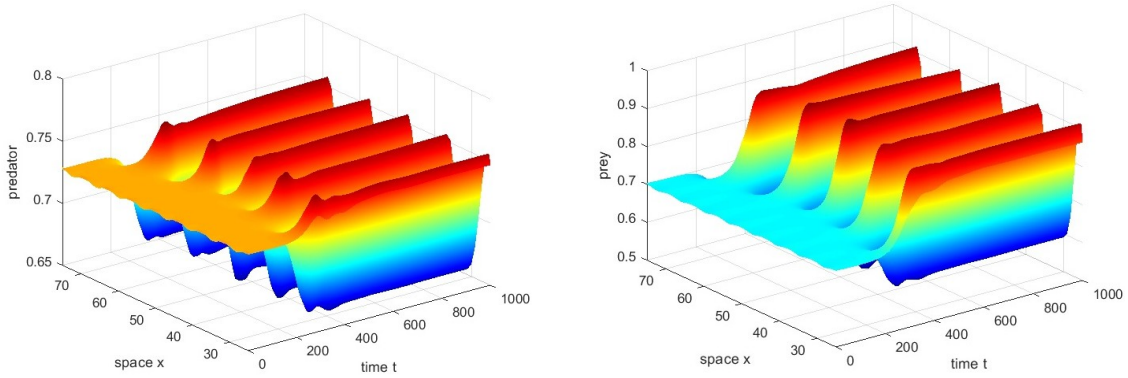

(a) (b)

Figure 7. The spatially nonhomogeneous steady patterns induced by the Turing bifurcation in system (1.2).

Next we continue to demonstrate the formation of the spatiotemporal patterns induced by the Turing-Hopf bifurcation in system (1.2). We take the parameter (ii) $d_1 = 0.2$, $d_2 = 2$, $s = 16$, $e = 1$, $d = 13$, $h = 4$, $r = 2$, $K = 1$, $a = 10$, $\tau = 0.9$, and $\chi = -5.2$ around the Turing-Hopf bifurcation onset $(\tau_c, \chi_{c1}) = (0.8, -4.8304)$. Numerical simulations indicate that system (1.2) does undergo spatiotemporal nonhomogeneous patterns caused by the Turing-Hopf bifurcation, as shown in Figure 8. The validity of Theorem 4.1 is verified.

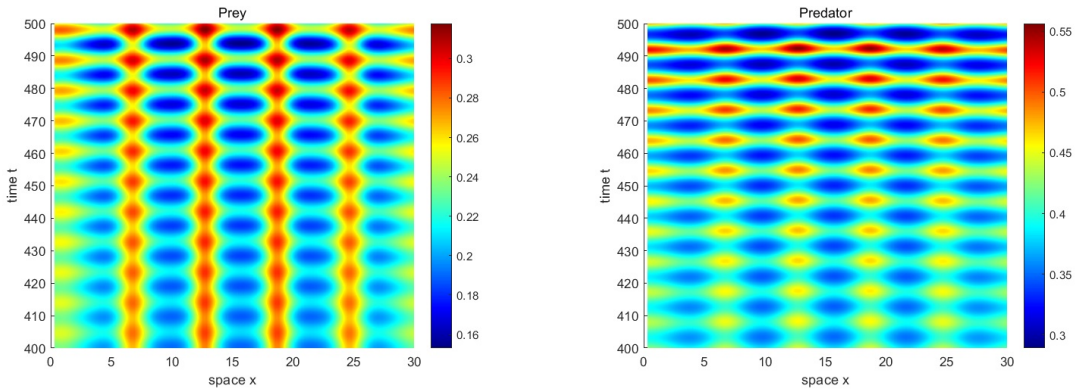

(a) (b)

Figure 8. The spatiotemporal nonhomogeneous patterns of system (1.2) induced by the Turing-Hopf bifurcation.

To perform the influence of the digestion delay control parameters τ, we choose the parameters (ii) $d_1 = 0.2$, $d_2 = 2$, $s = 16$, $e = 1$, $d = 13$, $h = 4$, $r = 2$, $K = 1$, and $a = 10$ and fix $\chi = -5.1 < \chi_{c1}$. Let τ vary around the threshold $\tau_c = 0.8$. When $\tau = 0$, that is, there is no digestion delay in system (1.2),

only the spatial nonhomogeneous steady pattern appears, as shown in Figure 9(a). Then, we choose $\tau = 0.89 > \tau_c$, and the regular stripe pattern is broken. This means that system (1.2) will present a spatiotemporal nonhomogeneous pattern due to the Turing-Hopf bifurcation, as shown in Figure 9(b). Moreover, we further choose $\tau = 0.9$ and $\tau = 0.92$, and the nonhomogeneous steady patterns gradually become unstable since the parameter τ has moved away from the Hopf bifurcation threshold τ_c, as shown in Figure 9(c) and (d).

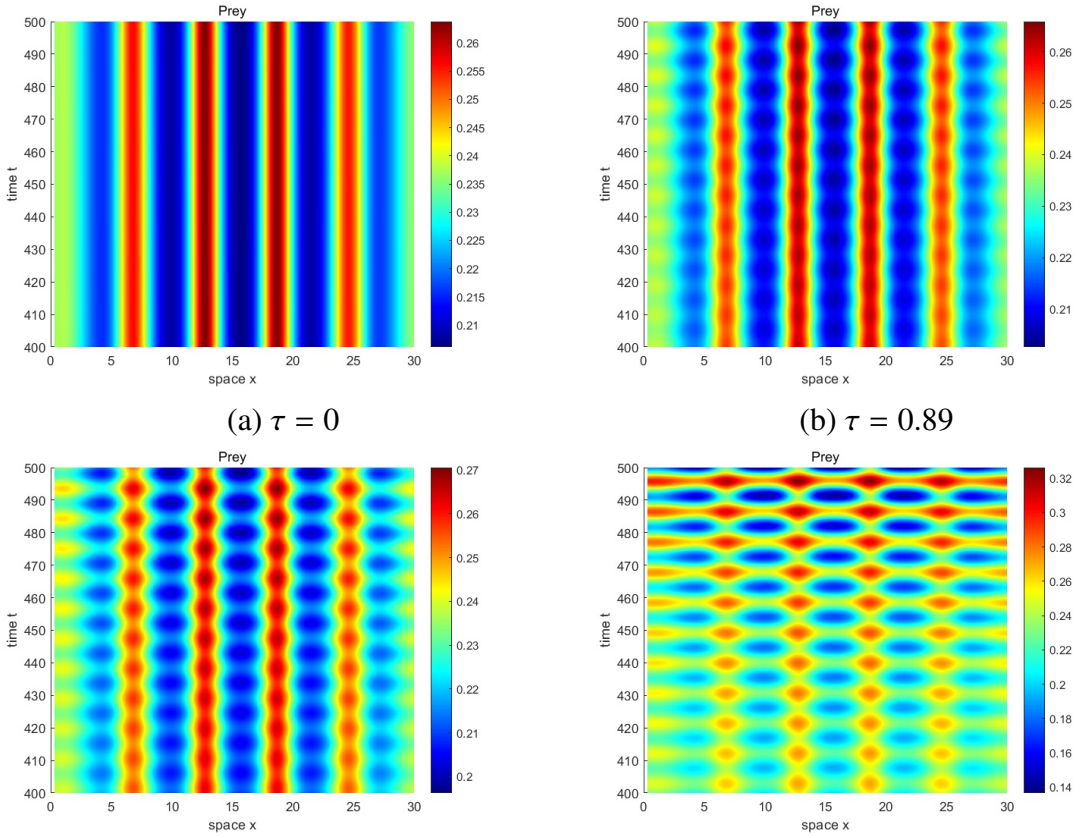

(a) $\tau = 0$ (b) $\tau = 0.89$

(c) $\tau = 0.9$ (d) $\tau = 0.92$

Figure 9. The spatial nonhomogeneous patterns with different digestion delay parameters τ.

We further choose the parameters (iii) $d_1 = 0.2$, $d_2 = 3$, $s = 1.5$, $e = 0.8$, $d = 1$, $h = 0.5$, $r = 1$, $K = 1.5$, and $a = 1$ and fix $\chi = -11.5 < \chi_{c1}$. Let τ vary around the threshold $\tau_c = 3.5156$. When $\tau = 0$, only the spatial nonhomogeneous steady pattern emerges, as shown in Figure 10(a). Next, we choose $\tau = 3.6 > \tau_c$, $\tau = 3.8$, and $\tau = 4$, respectively, and the regular stripe patterns are broken. The system (1.2) presents spatiotemporal nonhomogeneous periodic patterns due to the Turing-Hopf bifurcation, as shown in Figure 10(b)–(d). Overall, Figures 9 and 10 show the influence of the digestion delay parameter τ on the formation of the spatiotemporal nonhomogeneous periodic pattern of system (1.2).

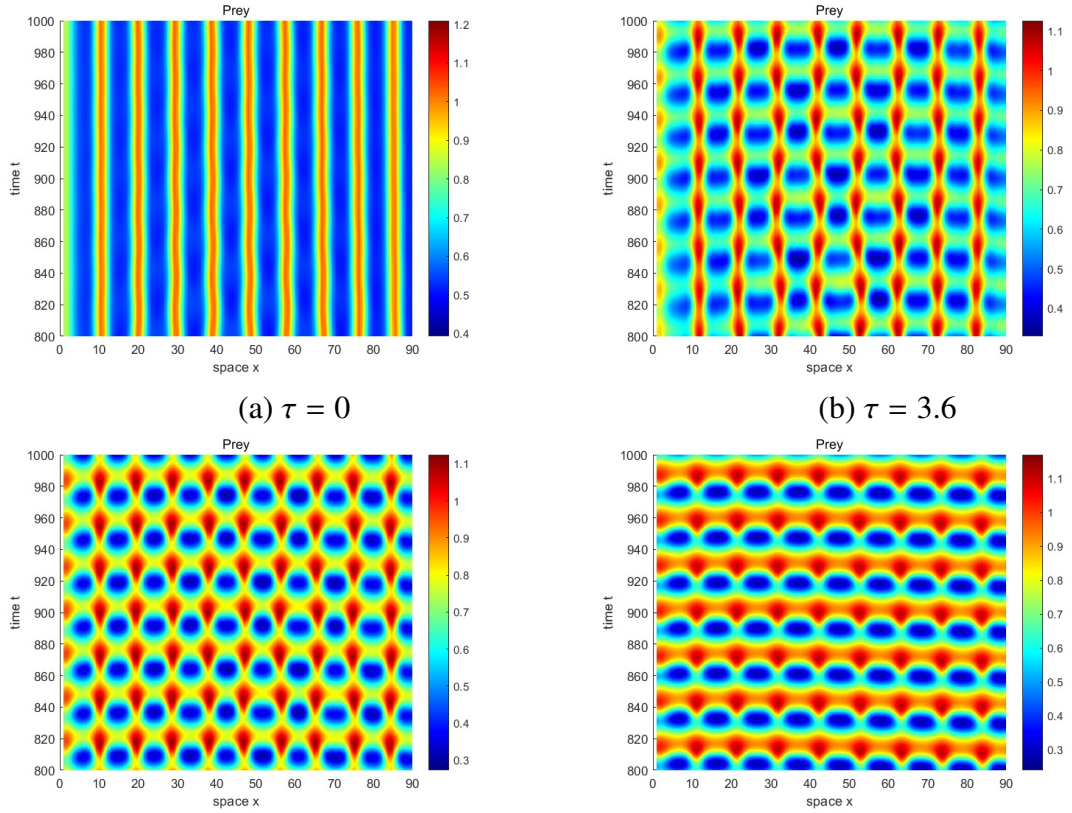

(a) $\tau = 0$ (b) $\tau = 3.6$

(c) $\tau = 3.8$ (d) $\tau = 4$

Figure 10. The spatial nonhomogeneous patterns with different digestion delay parameters τ.

Next, to perform the influence of the predator-taxis sensitive parameter χ, we continuously display the spatiotemporal pattern formation of system (1.2). We choose the parameter (ii) $d_1 = 0.2$, $d_2 = 2$, $s = 16$, $e = 1$, $d = 13$, $h = 4$, $r = 2$, $K = 1$, and $a = 10$ and fix $\tau = 0.9 > \tau_c$. First, when $\chi = 0$, it is shown that there is no pattern formation in the bounded area, as shown in Figure 11(a). Next, we choose $\chi = -3$, and $-4.8304 = \chi_{c1} < \chi < \chi_{c2} = 8.0586$, and then the homogeneous pattern occurs, as shown in Figure 11(b). Moreover, if we choose $\chi = -5 < \chi_{c1}$, a mixed pattern will occur, as shown in Figure 11(c). When $\chi = -5.06$, $\chi = -5.1$, and $\chi = -5.2$, slightly different spatiotemporal nonhomogeneous periodic patterns are presented in Figure 11(d)–(f). It is notable that the predator-taxis sensitivity parameter χ plays a crucial role in the formation of the spatiotemporal nonhomogeneous pattern of system (1.2). By adjusting the ranges of the control parameters of time delay and predator-taxis, the combined effect of predator-taxis and digestion delay leads to the emergence of spatiotemporal nonhomogeneous periodic patterns.

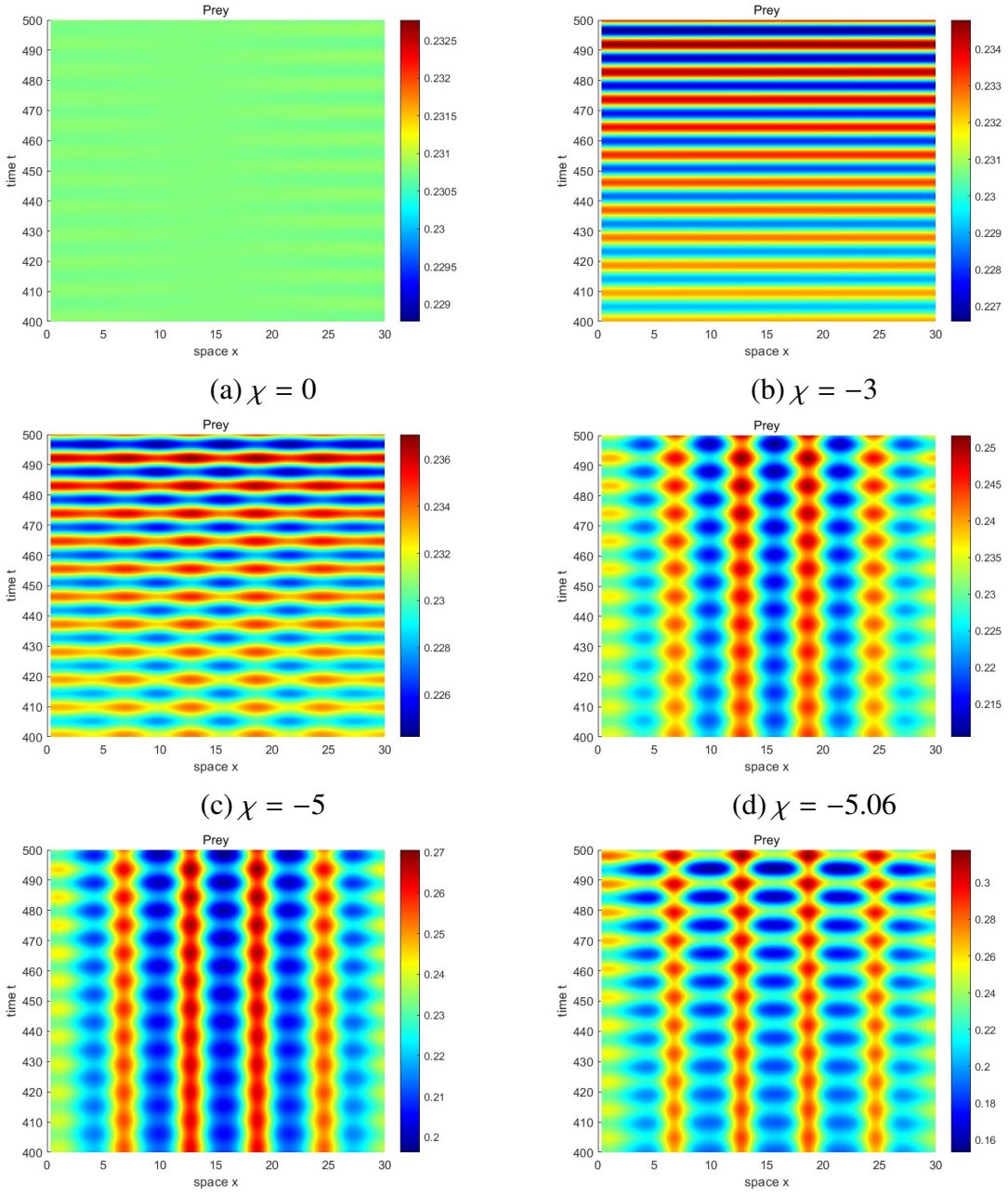

(a) $\chi = 0$ (b) $\chi = -3$

(c) $\chi = -5$ (d) $\chi = -5.06$

(e) $\chi = -5.1$ (f) $\chi = -5.2$

Figure 11. The spatial nonhomogeneous patterns with different predator-taxis sensitive parameters χ.

6. Conclusions

In this paper, we propose and study a modified Leslie-Gower model with predator-taxis and digestion delay under homogeneous Neumann boundary condition. Global stability for the positive equilibrium E_* without digestion delay is obtained, see Theorem 2.1. By considering the predator-taxis sensitive coefficient and digestion delay control parameter as bifurcation parameters, we establish

the occurrence conditions of the Hopf bifurcation and the Turing-Hopf bifurcation, see Theorems 3.1 and 4.1.

Numerical simulations confirmed the theoretical results, and spatiotemporal patterns of system (1.2) are observed, see Figures 2 and 3. In addition, the interaction of the spatially nonhomogeneous Hopf bifurcations with different modes leading to more complex dynamical phenomena which are known as a double Hopf bifurcation, see Figures 3(d) and 4. Furthermore, spatially nonhomogeneous steady patterns are observed near the Turing bifurcation critical point, see Figures 6 and 7, and spatiotemporal nonhomogeneous periodic patterns caused by Turing-Hopf bifurcation are shown in Figure 8. It is found that system (1.2) shows the spatially nonhomogeneous steady patterns and spatiotemporal nonhomogeneous periodic patterns with the change of the τ , see Figures 9 and 10. System (1.2) also exhibits the spatially homogeneous steady pattern, spatially homogeneous periodic pattern, spatiotemporal nonhomogeneous periodic pattern, and mixed pattern with the change of the predator-taxis sensitivity coefficient χ, see Figure 11. From the ecological point of view, spatial heterogeneity and periodic oscillation are universal in ecosystems, which mean they are nonhomogeneous in population spatial distribution and periodic fluctuations driven by time delay. Indeed, our numerical results have a realistic biological meaning.

Existing research shows that the predator-prey model without predator-taxis only has spatially homogeneous periodic solutions [30], and the predator-prey model without time delay only has stable spatially nonhomogeneous solutions [33]. However, the combined effect of predator-taxis and digestion delay leads to the spatiotemporal nonhomogeneous periodic patterns and other complex mixed patterns. This is an interesting dynamic phenomenon. The main results of this paper improve or extend some existing results. It further illustrates that the cognitive movement between the predator and prey can cause spatially heterogeneous distributions, even with a certain periodicity. Overall, the method presented in this paper can be applied to other time-delayed predator-prey models with taxis mechanism for the study of Turing instability, Turing-Hopf bifurcation, and the formation of spatiotemporal nonhomogeneous patterns.

Author contributions

Yan Meng: Methodology, Formal analysis, Investigation, Software, Supervision, Writing-review & editing, Writing-original draft; Jiaxin Xiao: Investigation, Methodology, Formal analysis, Software, Writing-original draft; Caijuan Jia: Writing-review & editing.

Use of Generative-AI tools declaration

The authors declare they have not used artificial intelligence (AI) tools in the creation of this article.

Acknowledgments

The authors are grateful to the handling editor and the anonymous reviewers for their reading and helpful suggestions to improve the quality of the present paper. This work is supported by National Natural Science Foundation of China (No. 12371481).

Conflict of interest

All authors declare that there are no competing interests.

References

1. A. J. Lotka, Relation between birth rates and death rates, *Science*, **26** (1907), 21–22.
2. V. Volterra, Variations and fluctuations of the number of individuals in animal species living together, *Journal du Conseil*, **3** (1928), 3–51. https://doi.org/10.1093/icesjms/3.1.3
3. X. Yan, Y. Li, G. Guo, Qualitative analysis on a diffusive predator-prey model with toxins, *J. Math. Anal. Appl.*, **486** (2020), 123868. https://doi.org/10.1016/j.jmaa.2020.123868
4. Y. Li, H. Liu, C. W. Lo, On inverse problems in predator-prey models, *J. Differ. Equations*, **397** (2024), 349–376. https://doi.org/10.1016/j.jde.2024.04.009
5. Y. Xing, W. Jiang, X. Cao, Multi-stable and spatiotemporal staggered patterns in a predator-prey model with predator-taxis and delay, *Math. Biosci. Eng.*, **20** (2023), 18413–18444. https://doi.org/10.3934/mbe.2023818
6. X. Yan, Y. Maimaiti, W. Yang, Stationary pattern and bifurcation of a Leslie-Gower predator-prey model with prey-taxis, *Math. Comput. Simulat.*, **201** (2022), 163–192. https://doi.org/10.1016/j.matcom.2022.05.010
7. W. Li, L. Zhang, J. Cao, A note on turing-hopf bifurcation in a diffusive leslie-gower model with weak allee effect on prey and fear effect on predator, *Appl. Math. Lett.*, **172** (2026), 109741. https://doi.org/10.1016/j.aml.2025.109741
8. C. Jia, Y. Meng, J. Xiao, Spatially nonhomogeneous patterns for a modified leslie-gower model with predator-taxis, *J. Comput. Appl. Math.*, **464** (2025), 116542. https://doi.org/10.1016/j.cam.2025.116542
9. M. E. Solomon, The natural control of animal populations, *J. Anim. Ecol.*, **18** (1949), 1–35. https://doi.org/10.2307/1578
10. R. Upadhyay, R. Agrawal, Dynamics and responses of a predator-prey system with competitive interference and time delay, *Nonlinear Dyn.*, **83** (2016), 821–837. https://doi.org/10.1007/s11071-015-2370-0
11. W. Li, W. Zhao, J. Cao, L. Huang, Dynamics of a linear source epidemic system with diffusion and media impact, *Z. Angew. Math. Phys.*, **75** (2024), 144. https://doi.org/10.1007/s00033-024-02271-2
12. W. Xu, H. Shu, Z. Tang, H. Wang, Complex dynamics in a general diffusive predator-prey model with predator maturation delay, *J. Dyn. Diff. Equat.*, **36** (2024), 1879–1904. https://doi.org/10.1007/s10884-022-10176-9
13. W. Li, L. Yang, J. Cao, Threshold dynamics of a degenerated diffusive incubation period host-pathogen model with saturation incidence rate, *Appl. Math. Lett.*, **160** (2025), 109312. https://doi.org/10.1016/j.aml.2024.109312

14. E. F. Keller, L. A. Segel, Model for chemotaxis, *J. Theor. Biol.*, **30** (1971), 225–234. https://doi.org/10.1016/0022-5193(71)90050-6

15. M. Banerjee, S. Ghorai, N. Mukherjee, Study of cross-diffusion induced turing patterns in a ratio-dependent prey-predator model via amplitude equations, *Appl. Math. Model.*, **55** (2018), 383–399. https://doi.org/10.1016/j.apm.2017.11.005

16. J. Wang, S. Wu, J. Shi, Pattern formation in diffusive predator-prey systems with predator-taxis and prey-taxis, *Discrete Cont. Dyn.-B*, **26** (2021), 1273–1289. https://doi.org/10.3934/dcdsb.2020162

17. X. Wang, X. Zou, Pattern formation of a predator-prey model with the cost of anti-predator behaviors, *Math. Biosci. Eng.*, **15** (2018), 775–805. https://doi.org/10.3934/mbe.2018035

18. P. Kareiva, G. Odell, Swarms of predators exhibit prey-taxis if individual predators use area-restricted search, *Amer. Nat.*, **130** (1987), 233–270. https://doi.org/10.1086/284707

19. M. Chen, Q. Zheng, Steady state bifurcation of a population model with chemotaxis, *Physica A*, **609** (2023), 128381. https://doi.org/10.1016/j.physa.2022.128381

20. M. Chen, Q. Zheng, Predator-taxis creates spatial pattern of a predator-prey model, *Chaos Soliton. Fract.*, **161** (2022), 112332. https://doi.org/10.1016/j.chaos.2022.112332

21. S. Wu, J. Wang, J. Shi, Dynamics and pattern formation of a diffusive predator-prey model with predator-taxis, *Math. Mod. Meth. Appl. Sci.*, **28** (2018), 2275–2312. https://doi.org/10.1142/S0218202518400158

22. H. Jin, Z. Wang, Global stability of prey-taxis systems, *J. Differ. Equations*, **262** (2017), 1257–1290. https://doi.org/10.1016/j.jde.2016.10.010

23. X. Wang, W. Wang, G. Zhang, Global bifurcation of solutions for a predator-prey model with prey-taxis, *Math. Method. Appl. Sci.*, **38** (2015), 431–443. https://doi.org/10.1002/mma.3079

24. Y. Li, J. Sun, Spatiotemporal dynamics of a delayed diffusive predator-prey model with hunting cooperation in predator and anti-predator behaviors in prey, *Chaos Soliton. Fract.*, **198** (2025), 116561. https://doi.org/10.1016/j.chaos.2025.116561

25. W. Shan, G. Ren, Dynamic behavior of taxis-driven intraguild predation model of three species with bd functional response, *Physica D*, **476** (2025), 134654. https://doi.org/10.1016/j.physd.2025.134654

26. Y. Lv, Influence of predator-taxis and time delay on the dynamical behavior of a predator-prey model with prey refuge and predator harvesting, *Chaos Soliton. Fract.*, **196** (2025), 116388. https://doi.org/10.1016/j.chaos.2025.116388

27. N. Almuallem, H. Mollah, S. Sarwardi, A study of a prey-predator model with disease in predator including gestation delay, treatment and linear harvesting of predator species, *AIMS Mathematics*, **10** (2025), 14657–14698. https://doi.org/10.3934/math.2025660

28. M. Mukherjee, D. Pal, S. Mahato, E. Bonyah, A. Shaikh, Analysis of prey-predator scheme in conjunction with help and gestation delay, *J. Math.*, **75** (2024), 2708546. https://doi.org/10.1155/2024/2708546

29. Y. Song, Y. Peng, X. Zou, Persistence, stability and hopf bifurcation in a diffusive ratio-dependent predator-prey model with delay, *Int. J. Bifurcat. Chaos*, **24** (2014), 1450093. https://doi.org/10.1142/S021812741450093X

30. S. Yao, J. Yang, S. Yuan, Bifurcation analysis in a modified Leslie-Gower predator-prey model with fear effect and multiple delays, *Math. Biosci. Eng.*, **21** (2024), 5658–5685. https://doi.org/10.3934/mbe.2024249

31. Y. Xing, W. Jiang, Turing-hopf bifurcation and bi-stable spatiotemporal periodic orbits in a delayed predator-prey model with predator-taxis, *J. Math. Anal. Appl.*, **533** (2024), 127994. https://doi.org/10.1016/j.jmaa.2023.127994

32. M. Chen, Spatiotemporal inhomogeneous pattern of a predator-prey model with delay and chemotaxis, *Nonlinear Dyn.*, **111** (2023), 19527–19541. https://doi.org/10.1007/s11071-023-08883-z

33. M. Chen, R. Wu, Dynamics of a harvested predator-prey model with predator-taxis, *Bull. Malays. Math. Sci. Soc.*, **46** (2023), 76. https://doi.org/10.1007/s40840-023-01470-w

AIMS Press

© 2025 the Author(s), licensee AIMS Press. This is an open access article distributed under the terms of the Creative Commons Attribution License (https://creativecommons.org/licenses/by/4.0)